Evaluación del Rendimiento de la Red 5G con Diferentes Implementaciones de Sistemas de Antenas Distribuidas en mmW para Zonas de Alto Tráfico en Interiores

Evaluation of 5G Network Performance with Different Distributed Antenna System Deployments for Indoor Hotspots at mmW

Autor: Alejandro Antón Ruiz

Tutor: Jose Francisco Monserrat del Río

Cotutora: Danaisy Prado Alvarez

Trabajo Fin de Grado presentado en la Escuela Técnica Superior de Ingenieros de Telecomunicación de la Universitat Politècnica de València, para la obtención del Título de Graduado en Ingeniería de Tecnologías y Servicios de Telecomunicación

Curso 2019-20

Valencia, 10 de septiembre de 2020

VLC/ CAMPUS VALENCIA, INTERNATIONAL CAMPUS OF EXCELLENCE

EMAS Gestión ambiental verificada REG.NO.ES-CV-000030

Resumen

En el contexto actual, en el que la sociedad se caracteriza por la gran cantidad de información disponible, una demanda creciente de contenidos a través de redes inalámbricas en interiores y el auge de las comunicaciones inalámbricas y móviles, es necesario explorar nuevas soluciones que permitan maximizar la capacidad de transmisión y minimizar el consumo de potencia en dicha transmisión.

Este trabajo final de grado consiste en una nueva propuesta de despliegue de puntos de acceso dentro de la tecnología 5G. Un nuevo despliegue basado en MIMO masivo sin celdas, que es un tipo concreto de sistema de antenas distribuidas, a la frecuencia de 60 GHz, perteneciente a la banda de las ondas milimétricas.

El caso analizado es una sala de reuniones de 60x60 m, con una mesa en el centro de 20x10 m, y 34 usuarios. Al ser un espacio diáfano, este escenario es idóneo, pues solamente ocurre propagación con línea de vista. El objetivo es lograr la máxima velocidad de descarga posible para todos los usuarios. Este trabajo final de grado evalúa el grado de cumplimiento de esta premisa para cuatro distribuciones de puntos de acceso distintas y para cuatro distintos escenarios. Estos escenarios incluyen movilidad o usuarios estáticos, así como la consideración de bloqueo de señal o no.

Los resultados muestran que hay dos distribuciones que rinden mejor que las demás y cuya elección dependerá de la preferencia entre mayor rendimiento medio, o un reparto más equilibrado de las capacidades de transmisión entre los usuarios.

Resum

En el context actual, en el qual la societat es caracteritza per la gran quantitat d'informació disponible, una demanda creixent de continguts a través de xarxes sense fils en interiors i l'apogeu de les comunicacions sense fils i mòbils, és necessari explorar noves solucions que permeten maximitzar la capacitat de transmissió i minimitzar el consum de potència en aquesta transmissió.

Aquest treball final de grau consisteix en una nova proposta de desplegament de punts d'accés dins de la tecnologia 5G. Un nou desplegament basat en MIMO massu sense cel·les, que és un tipus concret de sistema d'antenes distribuïdes, a la freqüència de 60 GHz, pertanyent a la banda de les ones mil·limètriques.

El cas analitzat és una sala de reunions de 60x60 m, amb una taula en el centre de 20x10 m, i 34 usuaris. A l'ésser un espai diàfan, aquest escenari és idoni, perquè solament ocorre propagació amb línia de vista. L'objectiu és aconseguir la màxima velocitat de descàrrega possible per a tots els usuaris. Aquest treball final de grau avalua el grau de compliment d'aquesta premissa per a quatre distribucions de punts d'accés diferents i per a quatre diferents escenaris. Aquests escenaris inclouen mobilitat o usuaris estàtics, així com la consideració de bloqueig de senyal o no.

Els resultats mostren que hi ha dues distribucions que rendeixen millor que les altres i l'elecció de les quals dependrà de la preferència entre major rendiment mitjà, o un repartiment més equilibrat de les capacitats de transmissió entre els usuaris.

Abstract

Nowadays, society is characterised by the vast amount of available information, a growing demand for content consumption in indoors through wireless networks, and mobile and wireless communications booming, so it is necessary to explore new solutions that enable the maximization of transmission capacity and the minimization of transmissions' power consumption.

This Bachelor's thesis consists in a new proposal of access points deployment within 5G technology. This deployment is based on cell-free massive MIMO, which is a particular type of distributed antenna system, at a frequency of 60 GHz, which belongs to the millimeter wave band.

The analysed use case is a 60x60 m meeting room, with a 20x10 m table in its centre, and 34 users. Due to the room being an open space, it is an ideal scenario, since only line-of-sight propagation occurs. The objective is to deliver as much download speed as possible to all users. The present work pretends to assess the degree of compliance with this premise for every one of the four APs distributions and for each of the four different considered scenarios. These scenarios include mobility or static users, as well as the consideration or lack thereof of signal body blockage.

Results show that there are two distributions which perform better than the rest and choosing between them will depend on the preference between higher average performance, or a more even distribution of transmission capabilities among users.

UNIVERSITAT
POLITÈCNICA
DE VALÈNCIA

_ TELECOM ESCUELA
TÉCNICA VLC SUPERIOR
DE INGENIERÍA DE
TELECOMUNICACIÓN

1 INTRODUCTION

1.1 CONTEXT

Nowadays, our society is characterised by information. Every day, approximately, a full Exabyte of data is generated [1]. With such a rate of data generation, powerful applications can be implemented, using, among other technologies, Big Data and Machine Learning, which have a vast amount of possibilities, such as personalised and predictive advertising, market segmentation, healthcare improvements, etc.

In order to access that information, communications are fundamental. They can be split into several categories, but one of the most relevant splits is the distinction between wired and wireless communications. With a prospective compound annual growth rate of 31% in mobile data traffic from 2019 (33 Exabytes a month) to 2025 (164 Exabytes a month) [2], it can be claimed that wireless communications are on the rise. The current coronavirus crisis has also highlighted how important communications are, and how much our modern societies depend on such communication.

Regarding wireless communications, two scenarios must be considered. In one hand, outdoors which require a wide area of coverage, moderate data rates, and have relatively low user density, but users' mobility is high [3]. On the other hand, indoors and outdoors where smaller coverage areas, higher data rates, and higher user density support are required, but users' mobility is lower. These scenarios are also known as hotspots, and their main aspect is that extremely high data rates must be handled by the system.

Specifically, indoor scenarios, as a recent survey suggest, will be where about 80% of wireless traffic will be consumed within the next years [4]. This suggests that deployments in these scenarios will become essential, helping to offload the deployments in outdoors that are designed with coverage over extreme data rates in mind.

Concerning data rates, there are three dimensions which, multiplied, result in the throughput (which is directly proportional to the data rate, being the effective part of it), namely bandwidth (B), spectral efficiency (SE) and average cell density (D) [5]. Therefore, improving one or more of these three dimensions will lead to higher data rates achievable by a certain deployment.

In respect of bandwidth, it is worth noting the scarcity of the resource it comes from: radioelectric spectrum. In addition, wherever it is licensed, it is extremely expensive, so the search for large bandwidths ends up in unlicensed bands. Moreover, if a vast amount of unlicensed spectrum is desired, it is necessary to resort to mmWave bands (30-300 GHz), where, for instance, there are 14 GHz of continuous unlicensed spectrum [6]. The main drawbacks for mmWave frequencies are higher pathloss, severe shadow fading and higher noise levels (assuming that higher B is used in mmWave, since noise is proportional to B), which all impact in SINR and, therefore, in the achievable (stable) SE.

When it comes to improving spectral efficiency (SE), one way it has been tackled is by increasing the number of antennas (M) per base station (BS), which increases SE, that is proportional to the signal-to-interference-plus-noise-ratio (SINR), due to the fact that "the BS can process its received signal over the array to selectively increase the signal gain without collecting more interference"[5], although such increase is not linear, since it corresponds to the binary logarithm of M. This increase in the number of antennas is easier in case of using mmWave frequencies, since antennas are sized proportionally to the wavelength.

Another improvement in SE can be achieved by serving multiple (K) user equipments (UEs) per cell, using space-division multiple access (SDMA), which, provided that the M/K ratio is a large number (4, 8 or more), leads to an almost K-fold improvement in total SE. Note that SE per user does not benefit from this, but the sum of all users' SE does and that [5]. This configuration can be deemed as multiple-input multiple-output (MIMO), where the inputs are the K UEs, and the outputs, the M antennas of the BS. Furthermore, a canonical definition of massive MIMO (mMIMO) is that it is a network which "uses a multicarrier TDD protocol. BS j is equipped with M_j antennas and serves K_j single-antenna UEs in each channel coherence block" [5]. Additionally, the M_j/K_j ratio must be higher than 1, and UEs can be equipped with multiple antennas, which can benefit from spatial multiplexing techniques to increase throughput.

Regarding average cell density, an obvious way to improve it is by increasing the number of cells or BSs, but this improvement has a limit, where the sum power of all the interfering signals from rest of BSs increases faster than it does the power of the desired signal [5]. Apart from that, excessive densification in indoor hotspot scenarios can be counter-productive, since it can cause UEs to be continuously switching between BSs if they move, which will cause increased signalling traffic and other undesired effects. Therefore, the approach of deploying multiple small cells (SCs) for indoor hotspot scenarios does not seem reasonable.

Considering the aforementioned points, it makes sense that the most sensible approach for indoor hotspot scenarios is cell-free mMIMO in mmWave. Cell-free implies that no cells (or BSs) are involved in the network, so intercell interference does not take place, resulting in the system not being interference bound [7]. It is worth noting that, when referring to the concept of cell-free mMIMO, a distributed antenna system is implied, since APs (antennas with RF chain) are distributed over the area where users are going to be served, which also helps lowering pathloss, thus increasing SE, and, therefore, improving throughput. The mMIMO approach somewhat compensates the SE losses resulting from operating with large bandwidths at mmWave frequencies. All this results in higher per-user and total throughput, which is the main objective to accomplish in indoor hotspot scenarios, outperforming systems based on small cells [7].

This is the framework where this bachelor's thesis belongs, since a system based on cell-free mMIMO is used in an indoor hotspot scenario, at a frequency of 60 GHz (mmWave).

1.2 STATE OF THE ART

In this Bachelor's thesis, a simulation of the performance of an indoor hotspot scenario, with a system based on one of 5G's solutions for such scenarios, cell-free mMIMO, which is in turn a distributed antenna system (DAS), at a mmWave frequency (60 GHz), is carried out. Then, a comparison between different distributions of the access points (APs) is conducted across four different situations, depending on considering or not user mobility and body blockage. It should be noted that only line-of-sight (LoS) propagation occurs, since the considered scenario is an open space.

The proposed use case can be framed in the enhanced mobile broadband (eMBB) use case defined in [8], where, for indoor hotspot scenarios, the objective is to provide a high data rate to all users, supporting a high density of them and pedestrian speeds mobility.

In order to achieve the objectives for this use case, there are three key technologies which, according to [9] should be implemented, namely ultra-dense networks (UDNs), leveraging the generous bandwidth at disposal in mmWave bands, and mMIMO antenna deployments. For this work, since the network comprises a single room, the concept of UDNs is not applicable, but the others are incorporated.

The evolution which has taken place from the cellular approach of traditional mobile networks to the concept here implemented, cell-free mMIMO, has been pretending to solve, one after the other, the inconveniences which the cellular approach has and the ones which have been arising from the evolutive process itself [7].

One such evolution was network MIMO or coordinated multipoint with joint transmission (CoMP-JT), where several base stations (BSs) serve a certain user. In order to limit the intercell interference, the serving BSs communicate with each other via backhaul link, resulting this in a coherently coordinated transmission (CCT), which achieves improvements in spectral efficiency (SE) similar to the improvement that will result from using multiple antennas in isolated scenarios [10]. Some drawbacks are the complex signal processing, which, in case of cell-free mMIMO, is much simpler, elevated backhaul overhead and costs of deployment [7].

Another evolution has consisted in shrinking the size of the cells, resulting in the small cells (SCs) deployments, which are based in deploying multiple SCs, consisting each one of them of APs that do not cooperate with the rest. However, in [11] SCs deployments are compared against cell-free mMIMO, resulting in cell-free mMIMO beating the performance obtained using SCs by a factor of 5 to 10, depending on whether the shadow fading is uncorrelated or correlated, respectively. It is worth noting that this comparison was performed for a frequency of 1.9 GHz.

Therefore, cell-free mMIMO is the logical next step forward after research over improving network performance, outperforming by a considerable margin the SCs systems [11] [12], as well as conventional mMIMO ones [13].

In respect of the mmWave band channel, simulation and modelling at 60 GHz for LoS and NLoS indoor scenarios have been conducted in [14], [15] (also considers 28, 39 and 73 GHz),

[16] (ray tracing is used), [17] (MIMO is considered and ray tracing used), [18] (statistical approach). The channel model used in the present work the one defined by 3GPP [19]. Channel capacity for LoS and NLoS indoor scenarios at 60 GHz has been calculated in [20].

When it comes to cell-free mMIMO, it has been compared against small cells in [11], [12] (different processing techniques for cell-free mMIMO are considered), its performance has been assessed in [21], [22] (a frequency of 1.9 GHz is used), power optimization and efficiency have been discussed in [23], [24] (cell-free mMIMO is one order of magnitude more efficient than co-located mMIMO), and favourable propagation and channel hardening discussed in [25], [26]. Different antenna layouts have been evaluated in [27].

Regarding body blockage in mmWave bands, it has been assessed in [28] (urban scenario, model evaluated using ray tracing), [29] (effects of body blockage from the perspective of a drone that carries a BS) and [30] (specifically for 60 GHz, empirical approach).

As for similar works to the present one, in [27] different DAS layouts (or distributions) have been compared, in the context of a mMIMO approach, which is also undertaken in the present work, but with the difference of not using arrays in any distribution and the frequency belonging to mmWave (60 GHz), whereas, in [27], the frequency used is 5 GHz.

Another somewhat similar work is [21], where distributed cell-free mMIMO (the same as DAS cell-free mMIMO) performance is assessed, across an indoor and an outdoor scenario, and comparing different power control strategies, all this at a frequency of 5.2 GHz, so it is not in the mmWave band, and the comparison is between power control strategies, not antenna distributions, but performance is assessed in a similar way and antenna distribution for the indoor scenario is comparable to one used in the present work.

To the best of the author's knowledge, the work presented in this Bachelor's thesis is the first one in which different APs distributions' performance is assessed, taking into account body blockage and user mobility concurrently, for indoor hotspot scenarios, using a distributed cell-free mMIMO system for a 5G network at 60 GHz (mmWave).

1.3 OBJECTIVES AND TASKS

The main objective of this Bachelor's thesis is to assess the performance of each of the proposed distributions in each scenario, so that relevant information can be derived about how each distribution performs against the rest, trying to answer the question of which distribution is the best performer overall, and case by case.

Moreover, gaining insights into how user mobility and body blockage affect each distribution is a major objective, as well as doing so into mmWave channel, cell-free mMIMO, body blockage and the rest of concepts involved in this work.

In addition, there are specific objectives, which are undertaken in order to achieve the main objective, namely:

- To evaluate the performance of different access points distributions for indoor hotspots.
- To consider different network deployments and their suitability based on different users' behaviour, based on their mobility.
- To analyse how body blockage affects the performance for each distribution.

In order to achieve the above-mentioned objectives and the realisation of this bachelor's thesis, different tasks have been accomplished, namely:

- Task 1: research on the state of the art of the topics related to the present work.
- Task 2: get used to the simulator, its structure, and parameters.
- Task 3: design and implement the use case scenario and APs distributions in the simulator.
- Task 4: implement user mobility in the simulator.
- Task 5: implement body blockage modelling in the simulator.
- Task 6: run the simulations with the parameters needed for each scenario and distribution.
- Task 7: choose the key performance indicators (KPIs) and build the custom figures and tables representing them, so relevant information can be derived.
- Task 8: draw conclusions and write final project report.

As it can be observed above, tasks are sequential, since previous ones are required to accomplish the next ones and, ultimately, they lead up to the achievement of the different objectives. Below, a Gantt diagram, representing the temporal distribution of the tasks:

Table 1. Temporal distribution of tasks

Task	Beginning	End	21-31 may	1-15 june	16-30 june	1-15 july	16-31 july	1-15 aug	16-31 aug	1-7 sep
1	21/05/2020	07/09/2020	■	■	■	■	■	■	■	■
2	09/06/2020	30/06/2020		■	■					
3	01/07/2020	31/07/2020				■	■			
4	16/07/2020	15/08/2020					■	■		
5	01/08/2020	15/08/2020						■		
6	16/08/2020	20/08/2020							■	
7	21/08/2020	26/08/2020							■	
8	16/08/2020	07/09/2020							■	■

1.4 ORGANIZATION OF THE DOCUMENT

In this section, a brief summary of the content of each of the main sections contained in this memory is undertaken:

1. **Introduction**: in this section, the context in which this bachelor's thesis is framed is defined, as well as how is the state of the art, what is new about this work and which are the objectives to achieve.
2. **Technological foundations**: here, the core technologies involved in the development of this work are described, so that the framework surrounding it is made clear.
3. **Methodology**: in this section, the use case is described, contributions of this bachelor's thesis are clarified and detailed, and simulation parameters and setups are defined. Therefore, the main specific aspects of this work are presented here, so the reader can identify its key features.
4. **Results and discussion**: here, results obtained from the simulations are conveniently shown, and comments and appreciations are made, deriving as much relevant information as possible.
5. **Conclusions and future research lines**: in this sections, conclusions taking into account the work as a whole are expressed, along with which future research should be advisable to do, so that further insights can be obtained, using as a base the work here developed.
6. **References**: here, all the consulted and cited documentation can be found, in an appropriate style, and sorted in order of appearance.

2 TECHNOLOGICAL FOUNDATIONS

2.1 CHANNEL AT MMWAVE FREQUENCIES

As it has been exposed in Section 1.1, mmWave bands are desirable due to the vast amount of unlicensed spectrum available, which permits large bandwidths to be used in communication systems, leading to higher throughputs, provided that SE, which depends on SINR, is not worsened enough to compensate for the use of such large bandwidths.

This SE worsening comes from various sources. One of them is noise, which increases with B, since it is a multiplying term in its formula (in linear units), as it can be observed below:

$$P_N(W) = k_B \left(\frac{J}{K}\right) * T(K) * B(Hz) \tag{1}$$

Another source is higher free space pathloss due to the higher frequency, and, therefore, lower wavelength, which leads to a lower signal received, worsening the SINR, and therefore lowering the coverage range, as it can be observed in the formula hereunder:

$$L_{free}(dB) = 20 * \log_{10}\left(\frac{4*\pi*d}{\lambda}\right) \tag{2}$$

In addition, propagation mechanisms are different when compared to lower frequencies ones, due to the smaller wavelength. In one hand, specular reflection is less likely to occur, since any imperfection of a material in the order of the wavelength (mm) leads to diffuse reflection, where rays are reflected in different directions. This leads to a scattered power reception [31]. On the other hand, diffraction across objects of tenths of meters or larger is blocked, causing large losses, due to the smaller first Fresnel zone (because of the smaller wavelength), which, for short distances, is within the range of centimeters. This leads to shadowing effects in presence of such objects, meaning that severe channel variations will take place, which can even lead to outages [32].

Another challenge to be faced is the increased Doppler spread that takes place at mmWave frequencies, being, at 60 GHz, twenty times the Doppler spread that takes place at 3 GHz [31]. For instance, at 60 km/h and 60 GHz, Doppler spread leads to a channel variation which overwhelms current cellular systems [33]. In order to reduce this effect, directional antennas and beamforming can help by reducing the angular spread, which lessens Doppler spread [34].

Furthermore, atmospheric absorption is higher at these frequencies, being 60 GHz a critical point, since O_2 absorption is maximum. However, atmospheric and rain absorption are in the range of a few dBs per kilometre [31], so it is almost negligible in short range deployments, like the one in the present work. This is not the case for building materials, because, for instance, a window introduces 40 or more dB of losses [32], so coverage in buildings is also a challenge.

To sum up, mmWave frequencies have the potential of reaching multi-gigabit throughputs [35], but there are challenges, which are inherent to the frequencies themselves, to be faced and solved in order to achieve such performances.

2.2 MASSIVE MIMO

As it has been stated in Section 1.1, massive MIMO (mMIMO) has been designed to increase spectral efficiency (SE). According to [5], "a Massive MIMO network is a multicarrier cellular network with L cells that operate according to a synchronous TDD protocol. BS_j is equipped with $M_j \gg 1$ antennas, to achieve channel hardening. BS_j communicates with K_j single-antenna UEs simultaneously on each time/frequency sample, with antenna-UE ratio $M_j/K_j > 1$. Each BS operates individually and processes its signals using linear receive combining and linear transmit precoding."

Therefore, mMIMO implies using a large number of antennas per BS, pursuing channel hardening, a phenomenon that results in the channel capacity not depending on small-scale fading, which in turn allows power allocation, interference management and scheduling to be undertaken in the time scale of large-scale fading, redounding in significant overhead savings compared to doing so in the time scale of small-scale fading [36].

In addition, in a hardened channel, no instantaneous channel state information is required by the receiver so that it can detect transmitted signals, being enough to know the statistical channel gains, which leads to less resources involved in channel estimation, namely power used during training phase and the length of it. In this case, where the statistical estimate of the channel gain is very close to the effective channel gain, downlink channel estimation can be avoided, so no downlink pilots are used, thus increasing throughput [36].

This high number of antennas also leads to another phenomenon called favourable propagation, which occurs when the channel vectors established between the BS and each UE are orthogonal (or almost). If this situation takes place, the sum-capacity of the system can be maximized, since inter-user interference is smaller [37].

Having an antenna-UE ratio greater than 1 means that there are more antennas per BS than users served by that BS, which enables efficient interference suppression and allows to use space-division multiple access (SDMA) to serve multiple user equipments (UEs) simultaneously, which leads to an improvement in total SE (per user SE remains unchanged comparing SDMA versus non SDMA) via multiplexing gain [5].

Operating with a time-division duplexing (TDD) protocol reduces the overhead generated in channel state information acquisition because of the use of numerous antennas, while allowing to distrust on parametrizable channel models, which, if could be made trustworthy, would enable frequency-division duplexing FDD operation [5].

It is worth noting that this concept is designed to be implemented in a conventional cellular fashion, where each BS serves a set of users within its reach, although there are other architectures based in this concept, such as network mMIMO, where several BSs serve one user, or cell-free mMIMO, where no cells exist.

Another point where this concept can vary is in the number of antennas that each UE has, which can be increased so that UEs can benefit from gains via spatial multiplexing. This

works by establishing independent transmission streams between each antenna in the UE and its BS counterpart, taking advantage of the fact that channels of each stream are different [38].

In summary, mMIMO enables SE improvements, as well as overhead and resource savings in channel estimation, which all contribute to achieving a higher system throughput and, in case multiple antennas per UE are used, per UE throughput can also be improved.

2.3 Cell-free Massive MIMO

As mentioned in Section 2.2, cell-free mMIMO is an implementation of the mMIMO concept, but in a cell-less fashion, so that there are no cell boundaries, resulting in no intercell interference and thus increasing performance. In this case, there is a considerably higher amount of access points (APs) than UEs, being these APs distributed over a wide area, and connected to the same central processing unit (CPU) via backhaul, controlling network synchronization, power allocation and data streams. Each AP and UE can have one or more antennas [7].

In a similar way to conventional mMIMO, TDD is the preferred duplexing method, since the overhead generated by it does not depend on the number of APs, depending only on the number of users, which means that more APs will not decrease performance due to more overhead, so performance will increase with the number of APs [7].

As stated in [39], cell-free mMIMO leads to "uniformly great service for everyone". This is due to the fact that, spreading a large amount of APs over an area implies that users will have several APs close to them, which redounds in lesser path losses, as well as more macro-diversity, resulting all this in higher and more evenly distributed per-user throughput.

Another advantage offered by cell-free mMIMO is its power efficiency, which can be achieved thanks to the distributed architecture, that makes possible to deliver power only to a subset of APs for each user without decreases in performance, which in turn increases power efficiency [7].

As also discussed in Section 2.2, favourable propagation occurs when there is a high number of APs, resulting in channel vectors established between the BS and each UE being orthogonal (or almost) and, owing to this phenomenon, higher SE can be achieved due to the lower inter-user interference. Moreover, as stated in [7]: "cell-free massive MIMO can achieve very good performance with simple linear processing such as maximum-ratio or zero-forcing processing. In addition, from the law of large numbers, uncorrelated noise and small-scale fading can be averaged out. Therefore, the system design (e.g., power controls and pilot assignments) depends only on the large-scale fading".

However, some challenges arise when implementing cell-free mMIMO. First, since all APs must be connected to the same CPU via backhaul, the system has to withstand a considerable amount of traffic and signalling. This problem can be tackled via a user-centric approach, so that a given UE is served by a subset of APs close to it that share a CPU, therefore existing several CPUs in the system, helping to relax the backhaul performance requirements significantly [40].

In addition, synchronization of such a large amount of APs, which have to serve UEs coherently, is, by any means, simple and must be tackled to achieve a low-cost solution [7]. Finally, due to the finite coherence time and the elevated number of users, it is not always possible to use pair wisely orthogonal uplink pilots for channel estimation for all UEs, so a phenomenon called pilot contamination can occur. In that case, UEs with non-orthogonal pilots will interfere to each other, resulting in correlated channel estimates, redounding in decreased performance [21].

To sum up, cell-free mMIMO implies several improvements in SE, power efficiency, overhead and signal processing complexity, although there are drawbacks as well, whose overcoming is key to unleash the full potential of this concept.

2.4 BODY BLOCKAGE

In Section 2.1 it has been mentioned that, due to the small wavelengths at mmWave frequencies, the first Fresnel zone for short distances is in the centimetre range. This makes that objects with a dimension within that range that obstruct first Fresnel zone will cause severe drops (which will revert when the object is no longer obstructing) in the received power, leading to the phenomenon known as shadowing.

Human body is not an exception when it comes to the ability of obstructing mmWave signals [41] and, due to the proximity of the user equipments (UEs) to the users themselves, it is very likely that human body blockage induced shadowing occurs. In that case, up to 20-25 dB of losses can be introduced at 60 GHz [42].

Therefore, when designing mmWave communication systems in which human beings are going to carry UEs, be in front of them (e.g. laptops) or simply be in between a direct path between a transmitter and a receiver, human body blockage effects should be taken into account, keeping in mind that not doing so will result in more severe inaccuracy the higher the frequency is.

UNIVERSITAT
POLITÈCNICA
DE VALÈNCIA

_ **TELECOM** ESCUELA
TÉCNICA **VLC** SUPERIOR
DE INGENIERÍA DE
TELECOMUNICACIÓN

3   METHODOLOGY

3.1   USE CASE

The proposed use case consists in a spacious meeting room with a hollow square setup [43], which is composed by a rectangular table in the middle of the room with, as its name suggests, an open space in its centre, where elements such as screens could be placed. The table has a seating capacity of 34 people, each of them with one user equipment (UE from hereon) or device, arranged in 11 per side in the x axis and 6 per side in the y axis. All this results, applying a 2 m per person space and a wideness of the table of 1 m, result in the outer dimensions of the table being 22 m (x axis) per 12 m (y axis), and the open space measuring 20 m (x axis) per 10 m (y axis).

When it comes to the meeting room's dimensions, according to the criteria of it being ample enough to allow mobility for its occupants, they result in 60 m (x axis) per 60 m (y axis), and a height of 4 m. In the following figure, the meeting room's layout can be observed:
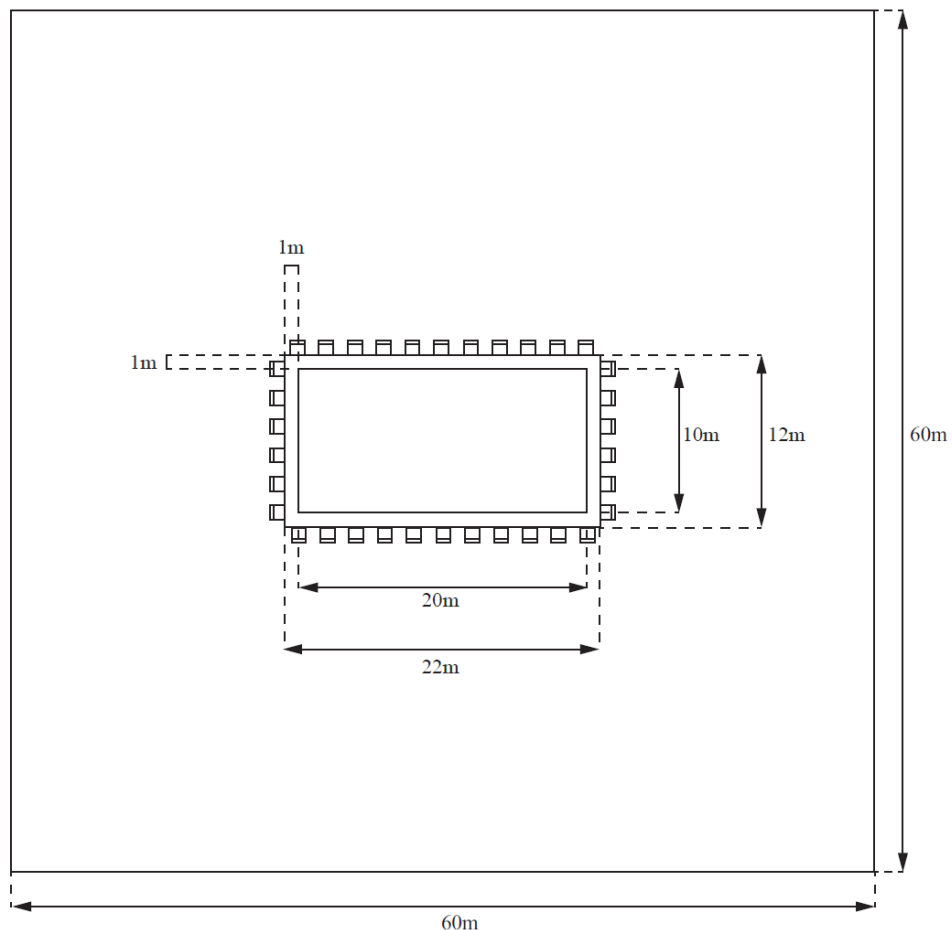

Figure 1. Meeting room's layout

According to the proposed scenario, the distribution of the users among the room will be twofold: all users seated (and therefore not moving) in their respective seats in the table (Figure 1), simulating the situation of a typical meeting; and all users moving through the room, excluding the space in which the table is placed, at a pace of 1.48 m/s [44], simulating this a break during the meeting or, for instance, a stand-up meeting.

The objective in this use case is that, with the proposed distributed antenna system (DAS), users can benefit from a seamless and smooth experience when using their devices, although, for the present work, only downlink performance is going to be evaluated.

Given the fact that the described room is an open space where many stationary or pedestrian users (as much as 34) coincide at the same time, the scenario is considered to be an indoor hotspot, as referred in [45].

This use case, although being abstract, could be translated to real life examples such as a shareholders meeting, a congress, or a boardroom meeting of a large company.

3.2 CONTRIBUTIONS TO THE SIMULATION TOOL

This Bachelor's Thesis takes as its base a mmWave indoor simulator developed by iTEAM Research Group and based in MATLAB, so it is necessary to clarify which contributions have been made here.

But first, a brief description of the simulator. As it has been mentioned, it is an indoor simulator, so it has the possibility of using several indoor channel models, namely InH_A, InH_B [45], and 3GPP InH Office [46], all of them belonging to the indoor hotspot use case. Additionally, LoS and NLoS implementations can be selected, as well as general parameters such as the frequency, the bandwidth of the resource block, the slot duration, or the number of users and how many of them can be served within a slot. Furthermore, different antenna array configurations can be selected, as well as diverse types of antennas, by making minor changes. Also, there are available several precoders such as zero forcing (ZF), maximum ratio transmission (MRT) and variations of them based on different power allocation schemes. Finally, multiple access points distributions can be selected, including deployments based on small cells, as well as cell-free.

In respect of the contributions to the simulator, user mobility has been added, with tunable parameters such as how long users are moving in the same direction, as well as the pace at which they move. It provides the position, and direction of motion of each user at a given time, which is useful for the rest of calculations, including body blockage modelling. It is worth noting that, accordingly to the proposed use case, user mobility has been implemented in a way that does not allow users to be in positions where the table and its hollow section are. The MATLAB implementation of the user mobility can be found, with the corresponding comments, in Section 7.1, as an annex.

Furthermore, body blockage modelling has been added, following the 3GPP recommendation [19]. From the two proposed models, the model B is the one selected, given

UNIVERSITAT
POLITÈCNICA
DE VALÈNCIA

_ **TELECOM** ESCUELA
TÉCNICA **VLC** SUPERIOR
DE INGENIERÍA DE
TELECOMUNICACIÓN

that it is capable of a more realistic and specific blocking modelling, based on its geometric approach. It is worth mentioning that, since the scenario is considered as indoor hotspot, only the section of the body blocking model which considers LoS condition has been implemented. Nevertheless, implementing the NLoS part of the blocking model is quite simple and could be carried out whenever there is a need to do so.

In this model, users are modelled as blockers in a rectangular shape, with a width of 0.3 m and a height of 1.7 m when standing up and, as a modification to the model introduced here, a height of 1.31 m when seated (average between men's and women's average seated height) [47]. With that in mind, the screens which model the users are rotated for each angle of arrival (AoA), in such a manner that they are perpendicular to it, and then four distances per each of the two views (top and side) are calculated: $D1_{w1}$, $D1_{w2}$, $D2_{w1}$, $D2_{w2}$ for the top view (parallel to the ground plane) and $D1_{h1}$, $D1_{h2}$, $D2_{h1}$, $D2_{h2}$ for the side view (perpendicular to the ground plane). It can be observed in a clearer way in the following figure:
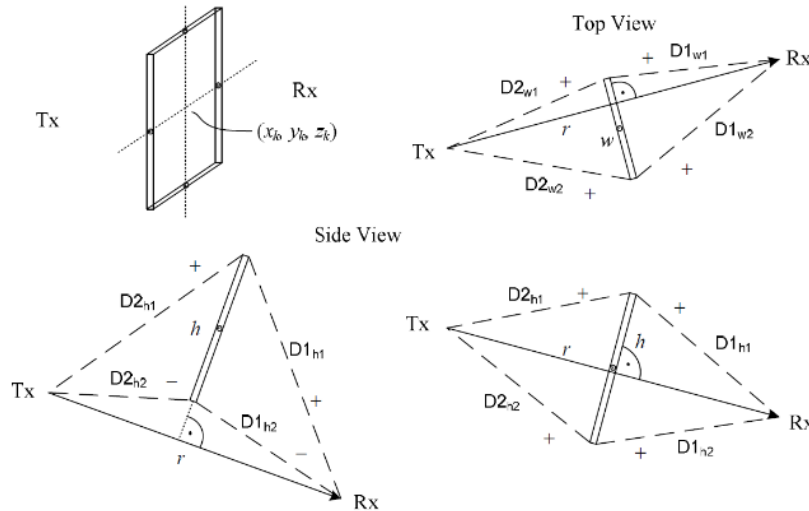

Figure 2. Geometric relation among blocker, receiver and transmitter. Source: [19]

Afterwards, knife-edge diffraction values at each of the four edges of the screen that models users are obtained using an equation with a varying sign depending on whether or not the screen is intercepted by the transmitter to receiver path. The equation can be observed here (note that r stands for the distance between transmitter and receiver for each view):

$$F_{h1|h2|w1|w2} = \tan^{-1}\left(\pm\frac{\pi}{2}\sqrt{\frac{\pi}{\lambda}}(D1_{h1|h2|w1|w2} + D2_{h1|h2|w1|w2} - r)\right) \quad (3)$$

Finally, total body blockage losses for each AoA and combination of user and access point is obtained following this equation:

$$L_{bb}(dB) = -20\log_{10}(1 - (F_{h1} + F_{h2})(F_{w1} + F_{w2})) \quad (4)$$

14

This body blockage model is integrated within the rest of the blocks in which the simulator is divided, as it can be observed in the following figure:
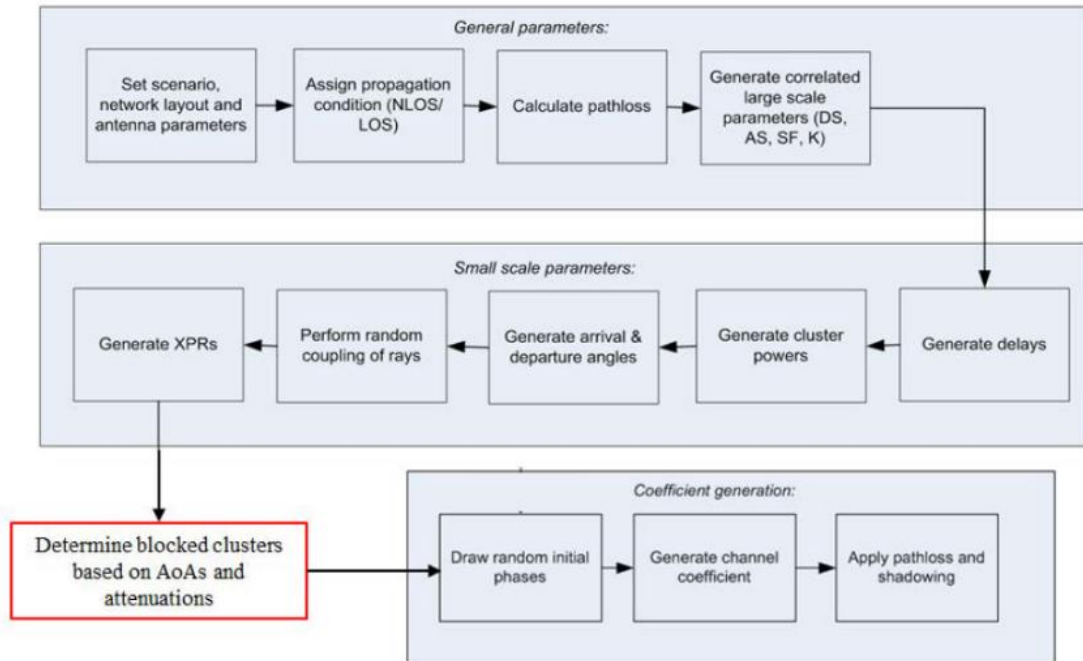

Figure 3. Channel generation blocks and procedure with body blockage model. Source: [19]

The MATLAB implementation of this body blockage model can be found, with the corresponding comments, in section 7.2, as an annex.

Lastly, the different APs distributions that have been proposed for this use case (see section 3.4) have been implemented, taking into account the dimensions of the scenario, as well as, in some cases, the dimensions of the table. Such distributions could be used, with minor adjustments for some of them, in scenarios with different dimensions for the room itself as well as for the table.

3.3 SIMULATION PARAMETERS

The simulator is configured with a series of parameters. For practical reasons, only relevant parameters are going to be mentioned. It is worth noting that the channel model used is the one from the ITU recommendation M.2412-0, specifically, the one named as InH_B, recommended for indoor hotspot scenarios [45].

UNIVERSITAT
POLITÈCNICA
DE VALÈNCIA

_TELECOM ESCUELA
TÉCNICA VLC SUPERIOR
DE INGENIERÍA DE
TELECOMUNICACIÓN

Table 2. Simulation main parameters

Parameters	Value
Carrier frequency (f_c)	60 GHz
Bandwidth (B)	80 MHz
Coherence interval length (τ_c)	200 samples
Training phase length (τ_p)	20 samples
Useful bandwidth (Useful B)	72 MHz
DAE height	4 m
UE height	1.5 m standing/0.7 m seated [47]
DAE maximum transmit power	23 dBm
Number of antennas at each DAE	1
Number of antennas at each UE	1
Type of DAE antenna	Omnidirectional
Type of UE antenna	Omnidirectional
UE motion speed (when considering mobility)	5.328 km/h [44]
LoS/NLoS condition	LoS for every setup
Modulation	OFDM
Receiver type	MMSE
Power control scheme	Channel-dependent full power transmission

3.4 SIMULATION SETUPS

In this section different configurations for the simulator are proposed. They account for a total of four distributions of the APs, along with four possible scenarios for each distribution. Before the table which can be found below (Table 3), some notes about the distributions and scenarios must be made:

- Distributions (see Figures 4 to 6, below Table 3):
  - Uniform distribution (UNIFORM from now on) (Figure 4) / true uniform distribution (TUNIFORM from hereon) (Figure 5): APs are distributed evenly among the room, including (TUNIFORM) or not (UNIFORM) the hollow section, with a certain separation between APs, which is halved when it comes to the distance between the APs and the borders of the room, as well as the borders of the hollow section.
  - Edge distribution (EDGE from here on): APs are distributed along the borders of the room (Figure 6).
  - Double Edge distribution (DOUBLE_EDGE from now on): APs are distributed along the borders of the room, as well as along the borders of the table's hollow section (Figure 7).
- APs separation: defines a separation (in meters) between APs, which, when it comes to the separation between APs and borders, it is halved.
- User mobility (MOB/STC): indicates which user distribution scenario is selected between the two possibilities of all users seated around the table, motionless (STC, from static), and users moving randomly through the room (except for the table) (MOB), which will

also affect the considered height of the users and UEs, resulting in different body blockage model parameters, among other things.

- Body blockage: indicates if body blockage modelling is applied.
- Number of APs denotes how many APs are placed in each distribution. Note that all distributions use the same number, for making the comparisons fairer, except for the UNIFORM one, just because it is a variant of TUNIFORM without APs placed in the hollow section.

Table 3. Setups specifications

| Code name	Distribution	APs separation (m)	User mobility	Body blockage	UE height (m)	Body height (m)	Number of APs
UNIFORM STC BB	Uniform	5	No	Yes	0.7	1.31	136
UNIFORM STC NO BB	Uniform	5	No	No	0.7	1.31	136
UNIFORM MOB BB	Uniform	5	Yes	Yes	1.5	1.7	136
UNIFORM MOB NO BB	Uniform	5	Yes	No	1.5	1.7	136
TUNIFORM STC BB	True Uniform	5	No	Yes	0.7	1.31	144
TUNIFORM STC NO BB	True Uniform	5	No	No	0.7	1.31	144
TUNIFORM MOB BB	True Uniform	5	Yes	Yes	1.5	1.7	144
TUNIFORM MOB NO BB	True Uniform	5	Yes	No	1.5	1.7	144
EDGE STC BB	Edge	1.62	No	Yes	0.7	1.31	144
EDGE STC NO BB	Edge	1.62	No	No	0.7	1.31	144
EDGE MOB BB	Edge	1.62	Yes	Yes	1.5	1.7	144
EDGE MOB NO BB	Edge	1.62	Yes	No	1.5	1.7	144
DOUBLE EDGE STC BB	Double edge	2.14 (exterior) 1.82 (hollow x) 2 (hollow y)	No	Yes	0.7	1.31	144
DOUBLE EDGE STC NO BB	Double edge	2.14 (exterior) 1.82 (hollow x) 2 (hollow y)	No	No	0.7	1.31	144
DOUBLE EDGE MOB BB	Double edge	2.14 (exterior) 1.82 (hollow x) 2 (hollow y)	Yes	Yes	1.5	1.7	144
DOUBLE EDGE MOB NO BB	Double edge	2.14 (exterior) 1.82 (hollow x) 2 (hollow y)	Yes	No	1.5	1.7	144
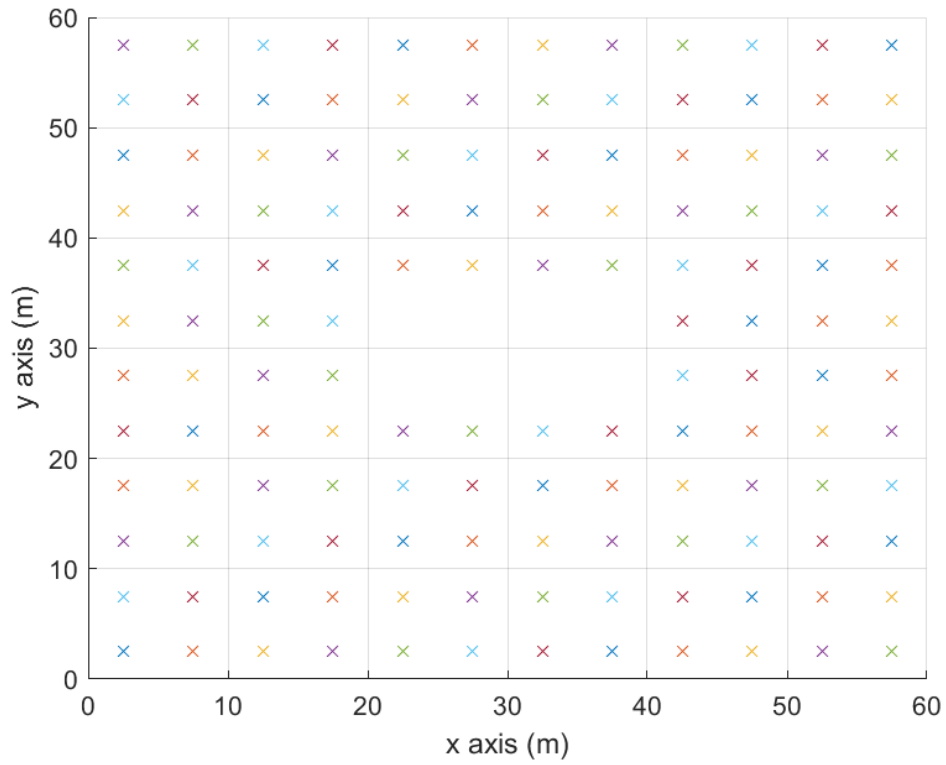
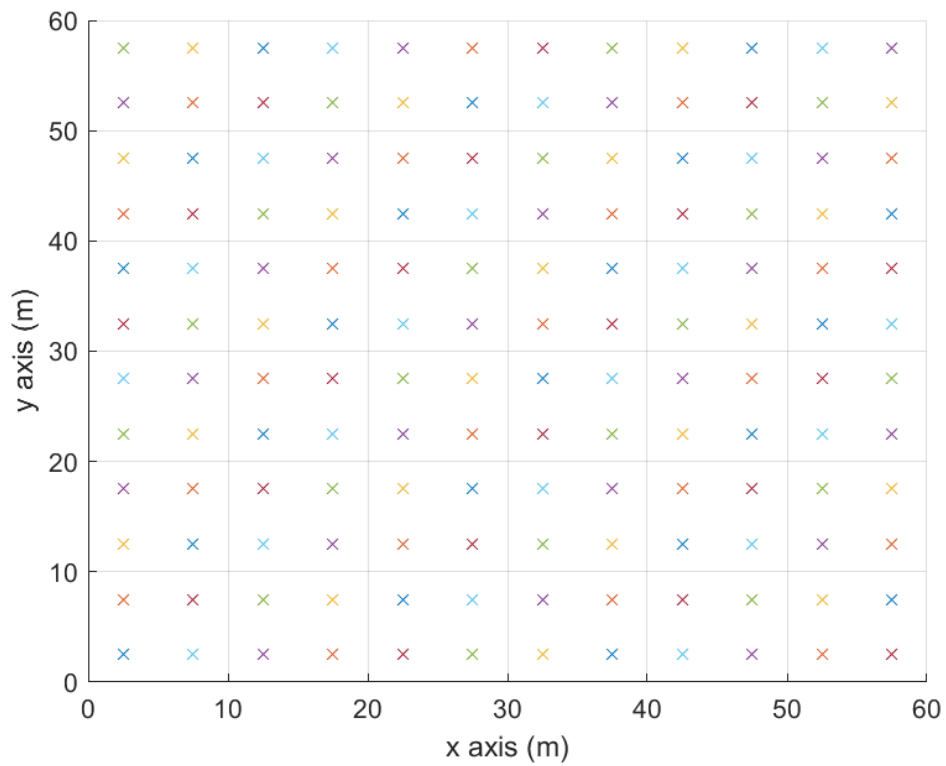*Figure 4. UNIFORM AP distribution*
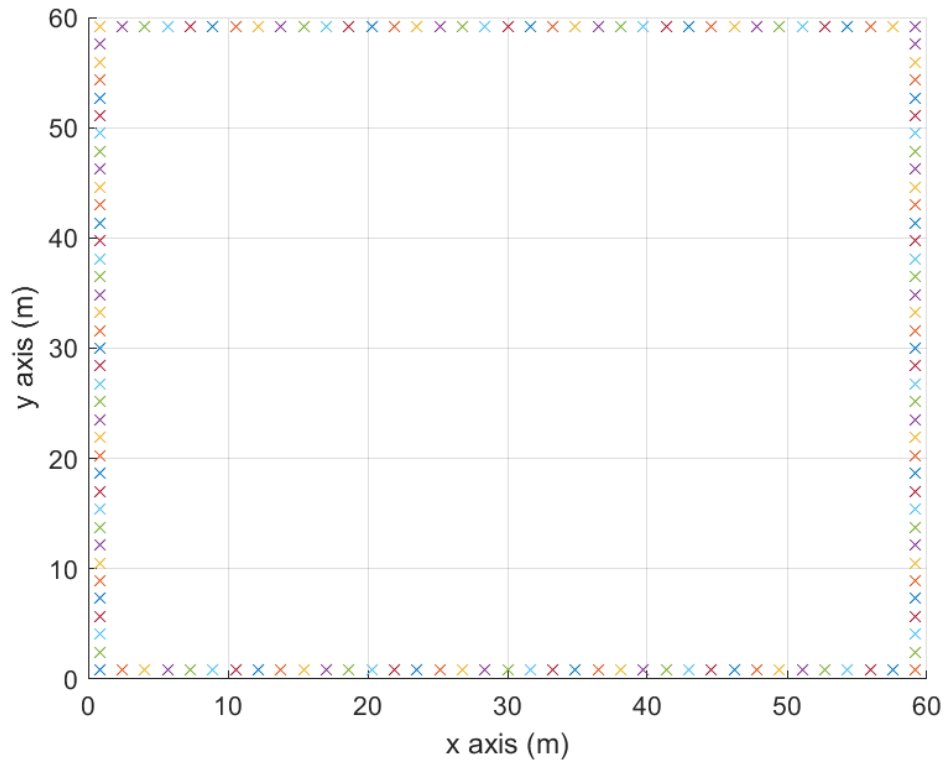

Figure 5. TUNIFORM AP distribution
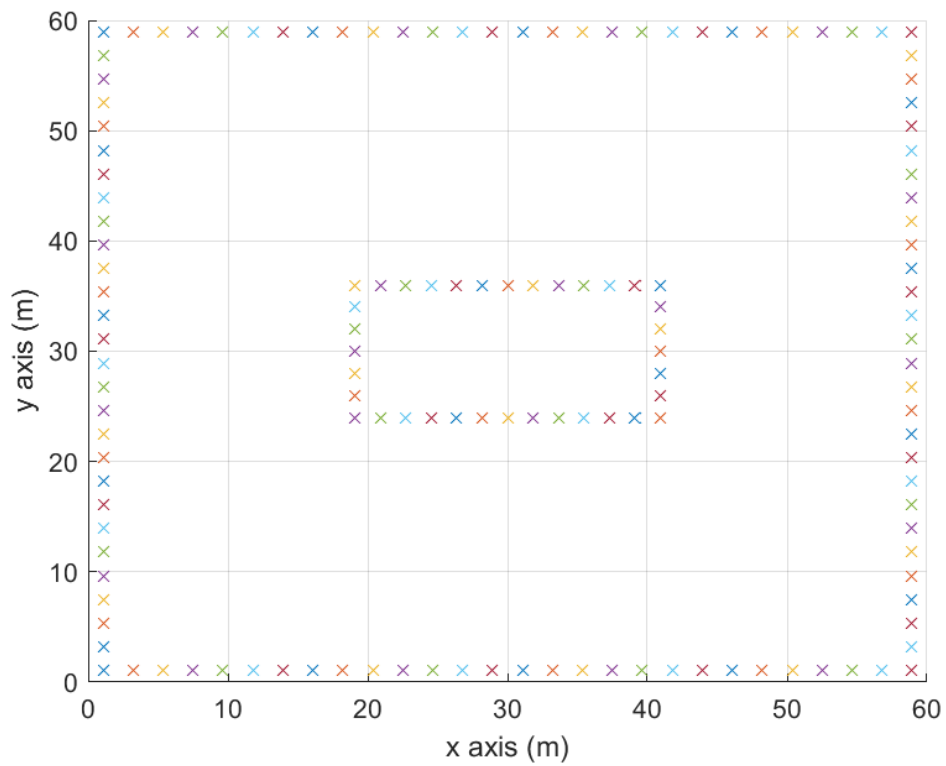
Figure 6. EDGE AP distribution

Figure 7. DOUBLE EDGE AP distribution

4   RESULTS AND DISCUSSION

4.1   KEY PERFORMANCE INDICATORS

In order to be able to compare and discuss how each of the proposed distributions performs in the different scenarios, it is necessary to establish how this performance is going to be assessed, which leads to the definition of the Key Performance Indicators (KPI from now on).

The first of the two chosen KPIs is Spectral Efficiency in downlink (SE from now on), which is calculated as follows (note that it has the scaling factor multiplying because it is the spectral efficiency for downlink):

$$SE_{Dl}\left(\frac{bit/_s}{Hz}\right) = Scaling\ Factor\ (Downlink) * log_2(1 + SINR) \tag{5}$$

$$Scaling\ Factor\ (Downlink) = \frac{\tau_c - \tau_p}{\tau_c} \tag{6}$$

The second KPI is the average throughput per user, in Mbps, which is calculated as follows:

$$AvgThr_{UE}(Mbps) = mean\left(SE_{Dl}\left(\frac{bit/_s}{Hz}\right) * B(Hz)\right)/10^6 \tag{7}$$

As it can be seen from the equations above, both KPIs are closely related (linearly, indeed). However, taking into account both the SE and the average throughput, it will be clear which part of the average throughput is due to the SE and which to the available bandwidth in mmWave band. Moreover, SE is going to be represented as a cumulative distribution function, showing the probability that an UE has a certain SE or less and, therefore, indicating how SE is distributed, the average throughput is going to show more of an overview of the overall performance of the system, enabling a simpler comparison between different results.

Another quality of the system which is going to be evaluated using SE is its "fairness", in terms of how SE is distributed among the users. This is relevant because, for a certain average throughput of the system, which can be interpreted as its performance, the distribution among the users of that performance may vary significantly, and, since average throughput and SE are linearly related, the distribution of SE represents how that performance is spread throughout the users, hence being capable of measuring the aforementioned "fairness" of the system.

As for KPIs representation, they are going to be both represented in plots, being the SE plot a regular one, while the average throughput's one is a bar plot. Each plot has the KPIs of several scenarios, in order to make the comparison between distributions and how they perform in each scenario meaningful, as is going to be seen in the next section.

4.2 PERFORMANCE COMPARISON FOR EACH SCENARIO

In this section, a comparison of how each distribution performs in each scenario is carried out. KPIs are presented in four different figures, each of them with a different scenario: static considering body blockage, static not considering body blockage, mobility considering body blockage, and mobility not considering body blockage. In each figure, the four different distributions are represented and, in order to be able to identify how every distribution performs in each scenario, compared to the rest of distributions.
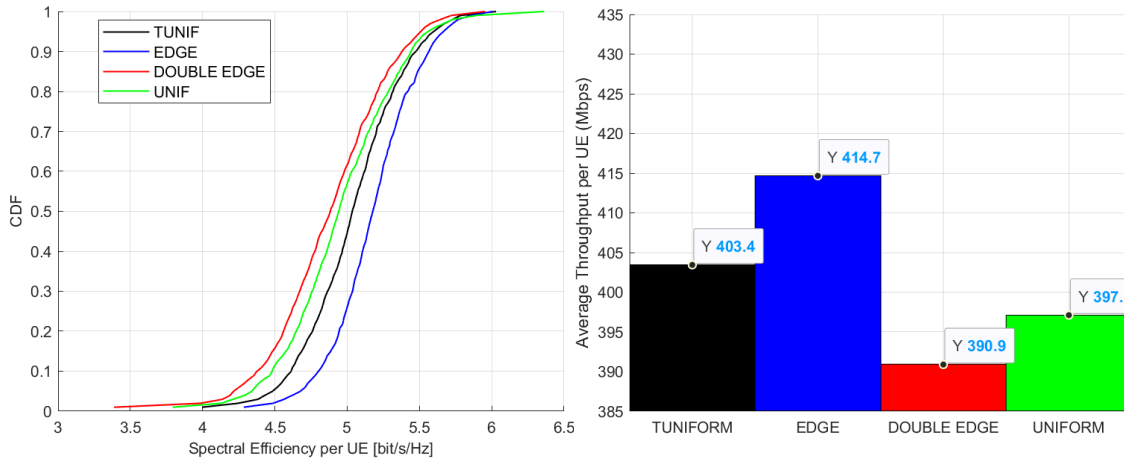

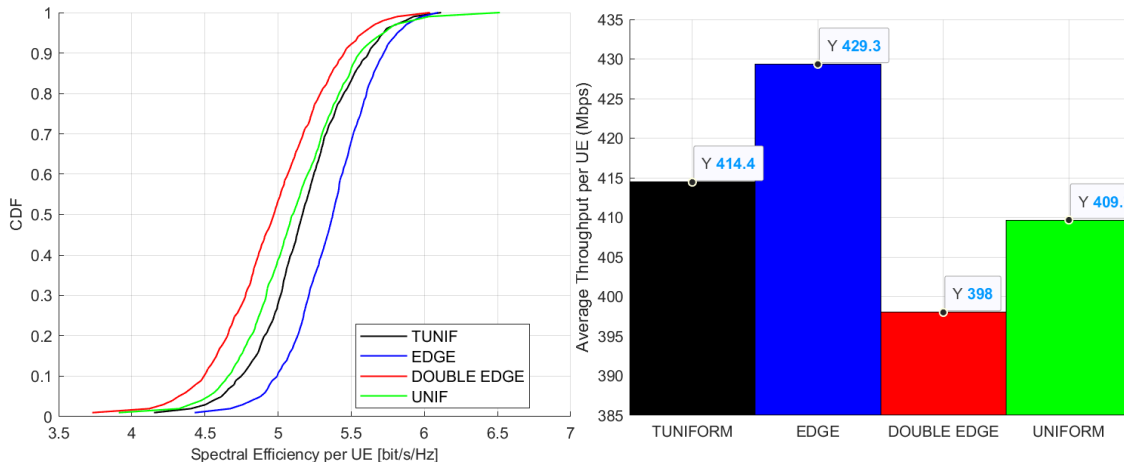*Figure 8. KPIs for Static Scenario considering Body Blockage*

Figure 9. KPIs for Static Scenario not considering Body Blockage

From the results above, there are some trends which should be highlighted. First, EDGE distribution clearly stands out over the rest of distributions in static scenarios, both in terms of average throughput per UE and SE, since, across all the CDF, EDGE distribution provides a higher SE, as it can be seen in Figures 8 and 9. Percentage increments of average throughput per UE for EDGE distribution range from 2.8% (versus TUNIFORM) to 6.1% (versus DOUBLE EDGE) when considering body blockage (Figure 8), and from 3.6% (versus TUNIFORM) to 7.86% (versus DOUBLE EDGE) when body blockage is not taken into account (Figure 9).

Contrary to the EDGE distribution, DOUBLE EDGE distribution is the worst performing one in static scenarios, both in terms of average throughput per UE and SE, being the latter worse for all the CDF, as can be observed in Figures 8 and 9. Percentage decreases of average throughput per UE for DOUBLE EDGE distribution range from 1.56% (versus UNIFORM) to 5.74% (versus EDGE) when considering body blockage (Figure 8), and from 2.86% (versus UNIFORM) to 7.3% (versus EDGE) when body blockage is not taken into account (Figure 9).
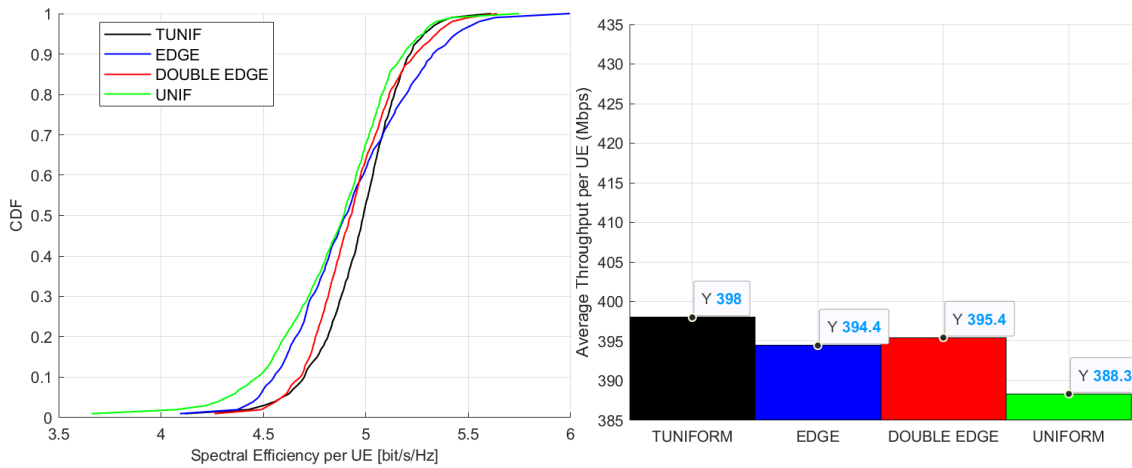

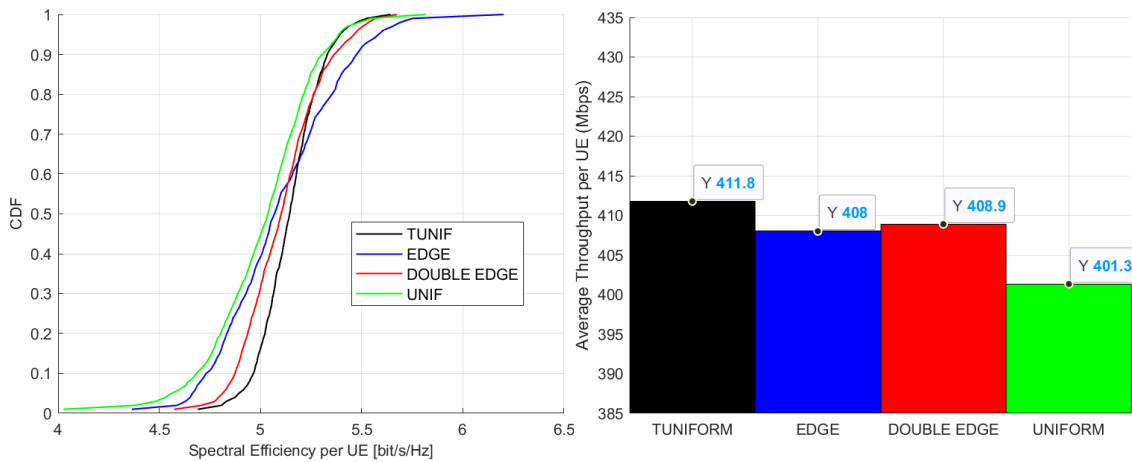*Figure 10. KPIs for Mobility Scenario considering Body Blockage*

Figure 11. KPIs for Mobility Scenario not considering Body Blockage

Another trend which can be identified is that UNIFORM distribution is clearly behind in both KPIs when mobility scenarios are concerned. Its SE is the lowest along all the CDF, and so is its average throughput per UE, as can be seen in Figures 10 and 11. When it comes to static scenarios, this distribution is only ahead from DOUBLE EDGE, being worse than both EDGE and TUNIFORM in both KPIs (Figures 8 and 9).

With respect to the TUNIFORM distribution, it is outperformed only by EDGE distribution in static scenarios for both KPIs (Figures 8 and 9) but, when mobility scenarios are taken into account, it stays ahead in terms of average throughput per UE, regardless of considering or not

body blockage. Nevertheless, in terms of SE, all of them perform similarly, except for UNIFORM, which, as mentioned above, which is outperformed by the rest in mobility scenarios (Figures 10 and 11).

However, there is an observable trend in the CDF of the SE for each distribution in mobility scenarios, being the curve steeper as the distribution gets more even (least even will be EDGE, then DOUBLE EDGE and, finally, TUNIFORM, being the most even), as it can be observed in Figures 10 and 11. A steeper curve means that the difference in SE between the users with a low SE and the ones with a high SE is smaller than the difference in a flatter curve. Thus, somehow, it can be regarded as a measurement of the "fairness" of the system, being the ideal system in terms of "fairness" one with an infinite slope of the SE CDF curve, which would imply that all users benefit from the same SE and, thus, the same performance, or, in other words, the same user experience.

As it can be observed in Figures 10 and 11, for mobility scenarios, the decision between EDGE, DOUBLE EDGE and TUNIFORM distributions is not crystal clear. On the one hand, average throughput per UE are fairly close, ranging the percentage decreases, in respect of TUNIFORM, of it from 0.65% (versus DOUBLE EDGE) to 0.9% (versus EDGE) when considering body blockage, and from 0.7% (versus DOUBLE EDGE) to 0.92% (versus EDGE) when not doing so. On the other hand, SE CDF curve is shaped differently depending on the distribution, being, as mentioned above, the steepest and, thus, "fairest", the one belonging to the TUNIFORM distribution, followed by the one from the DOUBLE EDGE distribution and, lastly, the flattest and "unfairest" curve, the one from the EDGE distribution.

All in all, taking into account the slight advantage in terms of average throughput per UE, and having the steepest and, therefore, "fairest" SE CDF curve (Figures 8 and 9), it stands to reason to state that TUNIFORM distribution is, by a not very wide margin, superior for mobility scenarios.

Nevertheless, when all scenarios are considered, both static and mobility ones, there is not any distribution which outperforms the rest in both cases, so trade-offs are involved in this decision. There are, however, just two sensible options, TUNIFORM and EDGE, since UNIFORM is the worst in mobility scenarios and the second worst in static ones, and DOUBLE EDGE, even if it is the second best in mobility scenarios for both KPIs, it is the worst in static ones, being outperformed in all cases by TUNIFORM distribution. Between TUNIFORM and EDGE, the decision will be based in whether EDGE's performance increase (2.8% in average throughput per UE when considering body blockage, and 3.6% when not, and across-the-board better SE) in static scenarios (Figures 8 and 9) compensates or not for the loss in "fairness" and the slight decrease in performance (0.9% in average throughput per UE when considering body blockage, and 0.92% when not) in mobility scenarios (Figures 10 and 11), when compared against the TUNIFORM distribution.

From another standpoint, distributions differ in their response to changes in the scenario, namely mobility/static and considering or not body blockage. These responses are shape changes and displacements of SE CDF curves, as well as variations in average throughput per UE, which, in case there is not a change in the shape of SE CDF curves, illustrates their

displacement. Down below, there is a figure containing the SE CDF curves for each distribution comparing how they change for each scenario:
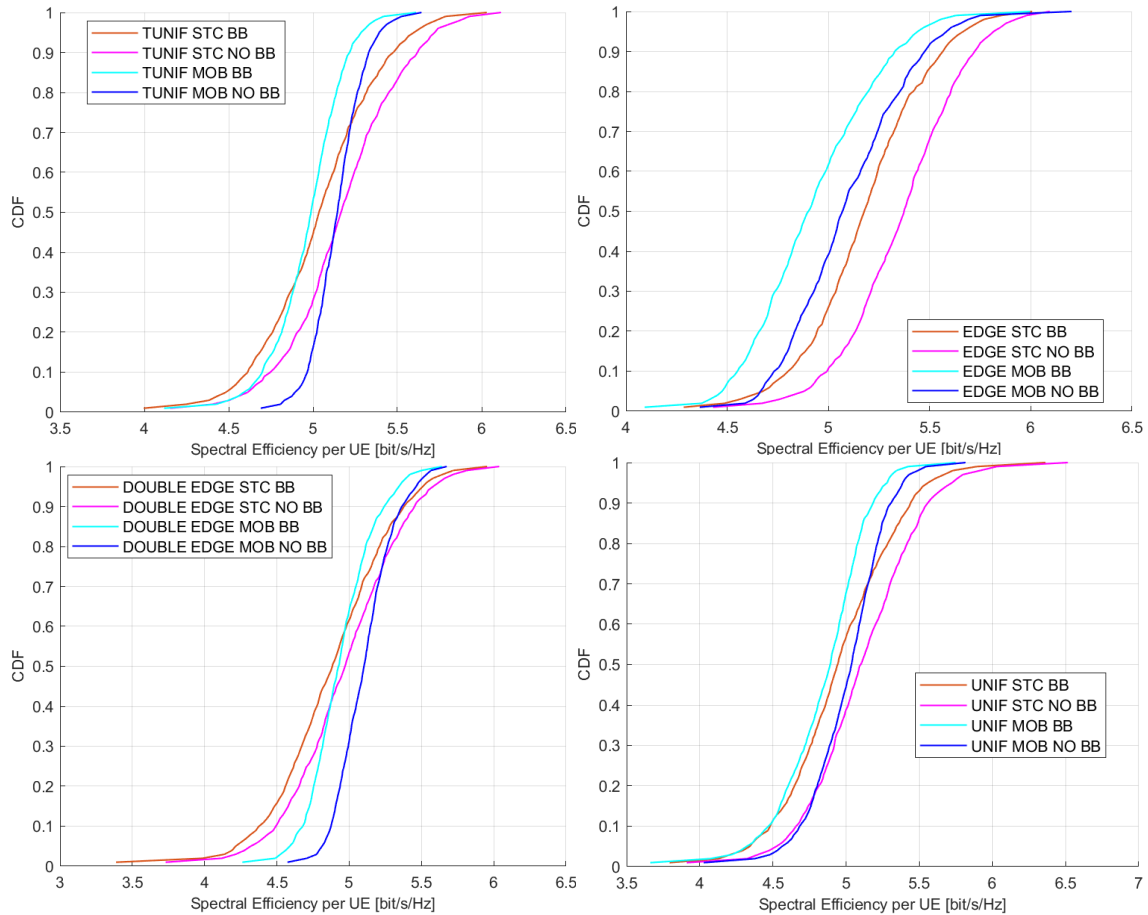

Figure 12. Spectral Efficiency curves of each distribution

With respect to the shape changes of SE CDF curves, there are some aspects worth mentioning, being the first of them that, as it can be seen in Figure 12, they only occur when switching between mobility/static scenarios, not taking place when switching between considering or not body blockage.

Another relevant point, which can be appreciated in Figure 12, is that EDGE distribution does not suffer any relevant changes in its SE CDF curve shape, whereas the rest of distributions follow another trend, which consists in SE CDF curves becoming steeper and, as mentioned before, "fairer" when switching from a static scenario to a mobility scenario, being this effect more intense in TUNIFORM and UNIFORM distributions.

Although the curves of the figure above show how performance is affected, they do not accomplish this task accurately or, at least, in a simple way. In order to illustrate as simply as possible how the different changes in the scenario affect to the performance of every distribution, the variation in average throughput per UE is assessed, with the help of the following table:

UNIVERSITAT
POLITÈCNICA
DE VALÈNCIA

_ **TELECOM** ESCUELA
TÉCNICA **VLC** SUPERIOR
DE INGENIERÍA DE
TELECOMUNICACIÓN

Table 4. Average throughput per UE variation comparison

	Average throughput per UE (Mbps) variation			
	TUNIFORM	EDGE	DOUBLE EDGE	UNIFORM
Static versus mobility (no body blockage)	0.63%	5.22%	-2.67%	2.09%
Static versus mobility (body blockage)	1.36%	5.15%	-1.14%	2.27%
No body blockage versus body blockage (static)	2.73%	3.52%	1.82%	3.17%
No body blockage versus body blockage (mobility)	3.47%	3.45%	3.41%	3.35%

From the table above, some relevant aspects can be identified, beginning with the fact that, as expected, considering body blockage leads to worse performance. This variation is similar in most cases, except for DOUBLE EDGE and, by a lower margin, TUNIFORM distributions in static scenarios.

In respect of static versus mobility scenarios, the trend for all distributions except por DOUBLE EDGE is that mobility scenarios decrease performance when compared to static ones, which happens the opposite way for DOUBLE EDGE. Apart from this, it is worth noting that EDGE distribution benefits the most, by a decent margin, from static scenarios, as can be observed in Table 4.

5 CONCLUSIONS AND FUTURE RESEARCH LINES

In this Bachelor's thesis, a performance evaluation of different APs distributions has been carried out, in the context of a cell-free massive MIMO system for an indoor hotspot scenario at 60 GHz (mmWave), taking into account user mobility and human body blockage, which is something that, as far as the author knows, has not been undertaken before.

The results show that, from the four proposed distributions, there are two that outperform the rest: TUNIFORM and EDGE. Choosing between them will depend on the designers' priorities: if static scenarios are the priority, then EDGE distribution will be the best implementation, whereas if mobility scenarios with slightly higher and more evenly distributed among users' throughput is the priority, then TUNIFORM distribution should be used.

In case there is no priority between static and mobility scenarios, then the decision will be based on whether the EDGE's 0.96% average increase in average throughput, in static and mobility scenarios in which body blockage is considered (more realistic), compensates for the poorer "fairness" for mobility scenarios in respect of TUNIFORM.

Another relevant point from the results is that, in this particular use case, in average, not considering human body blockage versus considering it leads to an increase in average throughput of 3.12%. This rather lower than expected performance impact can be due to the nature of cell-free mMIMO, because, since there are lots of APs in different positions, it is not very likely to obstruct a large enough number of them to lose significant performance.

Moreover, it is worth noting that EDGE distribution is, by a significant margin, the most affected because of the change from static to mobility scenarios and, conversely, DOUBLE EDGE distribution benefits from mobility scenarios.

With respect to future research lines, it will be interesting to opt for power control schemes different than the channel-dependent full power (CD-FPT) used here, as the ones used in [21], namely MMF (max-min fairness), MMF-RPB AP selection (max-min fairness power control with received-power-based AP selection) and MMF-CQB AP selection (max-min fairness power control with channel quality-based AP selection). In the last two cases, only a subset of APs is used to serve each user. Using these power control schemes could lead to steeper and thus "fairer" SE CDF curves, as well as higher average throughput, as results from [21] suggest.

Another future research line is simulating and measuring KPIs for uplink, since the present work only evaluates downlink performance.

Furthermore, the use of different type and number (arrays) of directive antennas in the APs constitutes a future research line, as well as using multi antenna configurations for UEs, since the small size of the antennas for mmWave frequencies makes those configurations not very costly.

Regarding the human body blockage model used, it has some limitations, since, in one hand, considers the human body a rotating rectangle, which, as a volume in revolution, ends up being a cylinder. This approach can be deemed as too simplistic. On the other hand, no

considerations about, for example, the hands or arms position and blockage they induce, which leads to significant variations in the introduced attenuation, as stated in [48].

Finally, since a frequency of 60 GHz is being used, and the main reason to choose such frequency is to dispose of large unlicensed bandwidths, in future research, it will be interesting to use bandwidths larger than the total 80 MHz used in the present work, in order to assess how much can a mmWave cell-free mMIMO benefit from using large bandwidths.

All in all, this Bachelor's thesis can be considered as a first step in the pursuit of an indoor hotspot solution that delivers excellent performance, not only by today's standards, which, in the humble author's opinion, are satisfied with the proposed solution, but also by future standards, where much higher throughputs will be required.

6 REFERENCES

[1] Bulao, Jacquelyn. "How Much Data Is Created Every Day in 2020?" [Online] 20th August 2020. [Cited: 1st September 2020.] https://techjury.net/blog/how-much-data-is-created-every-day/#gref.

[2] Ericsson. "Ericsson Mobility Report Junio 2020." [Online] June 2020. [Cited: 3rd September 2020.] https://www.ericsson.com/49e7b3/assets/local/mobility-report/documents/2020/emr-june2020-spanish.pdf.

[3] Zaidi, Ali & others. 5G Physical Layer: Principles, Models and Technology Components. 2018. p. 1-19.

[4] P. Gandotra, R. K. Jha and S. Jain, "Green Communication in Next Generation Cellular Networks: A Survey," in IEEE Access, vol. 5, pp. 11727-11758, 2017, doi: 10.1109/ACCESS.2017.2711784.

[5] Emil Björnson; Jakob Hoydis; Luca Sanguinetti, "Massive MIMO Networks: Spectral, Energy, and Hardware Efficiency," in Massive MIMO Networks: Spectral, Energy, and Hardware Efficiency, now, 2017.

[6] FCC. "Fact sheet: spectrum frontiers rules identify, open up vast amounts of new high-band spectrum for next generation (5G) wireless broadband." [Online] 2016. [Cited: 3rd September 2020.] https://transition.fcc.gov/Daily_Releases/Daily_Business/2016/db0714/DOC-340310A1.pdf.

[7] Ngo H.Q. (2018) "Cell-Free Massive MIMO." In: Shen X., Lin X., Zhang K. (eds) Encyclopedia of Wireless Networks. Springer, Cham. https://doi.org/10.1007/978-3-319-32903-1_137-1

[8] M. Shafi et al., "5G: A Tutorial Overview of Standards, Trials, Challenges, Deployment, and Practice," in IEEE Journal on Selected Areas in Communications, vol. 35, no. 6, pp. 1201-1221, June 2017, doi: 10.1109/JSAC.2017.2692307.

[9] S. A. Busari, S. Mumtaz, S. Al-Rubaye and J. Rodriguez, "5G Millimeter-Wave Mobile Broadband: Performance and Challenges," in IEEE Communications Magazine, vol. 56, no. 6, pp. 137-143, June 2018, doi: 10.1109/MCOM.2018.1700878.

[10] Foschini, Karakayali and Valenzuela, "Coordinating multiple antenna cellular networks to achieve enormous spectral efficiency," in IEE Proceedings - Communications, vol. 153, no. 4, pp. 548-555, August 2006, doi: 10.1049/ip-com:20050423.].

[11] H. Q. Ngo, A. Ashikhmin, H. Yang, E. G. Larsson and T. L. Marzetta, "Cell-Free Massive MIMO Versus Small Cells," in IEEE Transactions on Wireless Communications, vol. 16, no. 3, pp. 1834-1850, March 2017, doi: 10.1109/TWC.2017.2655515.

[12] E. Björnson and L. Sanguinetti, "Cell-Free versus Cellular Massive MIMO: What Processing is Needed for Cell-Free to Win?," 2019 IEEE 20th International Workshop on Signal Processing Advances in Wireless Communications (SPAWC), Cannes, France, 2019, pp. 1-5, doi: 10.1109/SPAWC.2019.8815488.

[13] P. Liu, K. Luo, D. Chen, and T. Jiang, "Spectral efficiency analysis of cell-free massive MIMO systems with zero-forcing detector," IEEE Trans. Wireless Commun., Feb 2020.

[14]   S. Li, Y. Liu, L. Lin, D. Sun, S. Yang and X. Sun, "Simulation and Modeling of Millimeter-Wave Channel at 60 GHz in Indoor Environment for 5G Wireless Communication System," 2018 IEEE International Conference on Computational Electromagnetics (ICCEM), Chengdu, 2018, pp. 1-3, doi: 10.1109/COMPEM.2018.8496691.

[15]   A. A. AlAbdullah, N. Ali, H. Obeidat, R. A. Abd-Alhmeed and S. Jones, "Indoor millimetre-wave propagation channel simulations at 28, 39, 60 and 73 GHz for 5G wireless networks," 2017 Internet Technologies and Applications (ITA), Wrexham, 2017, pp. 235-239, doi: 10.1109/ITECHA.2017.8101945.

[16]   A. Zhou, J. Huang, J. Sun, Q. Zhu, C. Wang and Y. Yang, "60 GHz channel measurements and ray tracing modeling in an indoor environment," 2017 9th International Conference on Wireless Communications and Signal Processing (WCSP), Nanjing, 2017, pp. 1-6, doi: 10.1109/WCSP.2017.8170934.

[17]   M. J. Kazemi, A. Abdipur and A. Mohammadi, "Indoor propagation MIMO channel modeling in 60 GHz using SBR based 3D ray tracing technique," 2012 Second Conference on Millimeter-Wave and Terahertz Technologies (MMWaTT), Tehran, 2012, pp. 25-28, doi: 10.1109/MMWaTT.2012.6532159.

[18]   M. A. Mou and M. M. Mowla, "Indoor mmWave Statistical Channel Model at V-Band for 5G Networks," 2019 5th International Conference on Advances in Electrical Engineering (ICAEE), Dhaka, Bangladesh, 2019, pp. 778-782, doi: 10.1109/ICAEE48663.2019.8975624.

[19]   3GPP TR 38.901. "Study on channel model for frequencies from 0.5 to 100 GHz." 2017.

[20]   D. Jie, J. Wang, H. Zhang and G. Wang, "Channel Capacity of 60 GHz Wireless Communication Systems over Indoor Line-of-Sight and Non-Line-of-Sight Channels," 2010 6th International Conference on Wireless Communications Networking and Mobile Computing (WiCOM), Chengdu, 2010, pp. 1-4, doi: 10.1109/WICOM.2010.5600924.

[21]   Interdonato, G., Björnson, E., Ngo, H. Q., Frenger, P., & Larsson, E. G. (2019). "Ubiquitous cell-free massive MIMO communications." EURASIP Journal on Wireless Communications and Networking, 2019(1), 197.

[22]   A. Papazafeiropoulos, P. Kourtessis, M. D. Renzo, S. Chatzinotas and J. M. Senior, "Performance Analysis of Cell-Free Massive MIMO Systems: A Stochastic Geometry Approach," in IEEE Transactions on Vehicular Technology, vol. 69, no. 4, pp. 3523-3537, April 2020, doi: 10.1109/TVT.2020.2970018.

[23]   E. Nayebi, A. Ashikhmin, T. L. Marzetta, H. Yang and B. D. Rao, "Precoding and power optimization in cell-free massive MIMO systems", *IEEE Trans. Wireless Commun.*, vol. 16, no. 7, pp. 4445-4459, Jul. 2017

[24]   H. Q. Ngo, L. Tran, T. Q. Duong, M. Matthaiou and E. G. Larsson, "On the total energy efficiency of cell-free massive MIMO", *IEEE Trans. Green Commun. Net.*, vol. 2, no. 1, pp. 25-39, Mar. 2018. J

[25]   Z. Chen and E. Björnson, "Channel hardening and favorable propagation in cell-free massive MIMO with stochastic geometry", IEEE Trans. Commun., vol. 66, no. 11, pp. 5205-5219, Nov. 2018.

[26]   S. Gunnarsson, J. Flordelis, L. Van der Perre and F. Tufvesson, "Channel Hardening in Massive MIMO-A Measurement Based Analysis," 2018 IEEE 19th International Workshop on Signal Processing Advances in Wireless Communications (SPAWC), Kalamata, 2018, pp. 1-5, doi: 10.1109/SPAWC.2018.8445925.

[27]   Y. Suzuki, T. Nishimura, T. Ohgane, Y. Ogawa and J. Hagiwara, "A Study on Layouts of Distributed Antenna Arrays in an Indoor Multi-User Massive MIMO System," 2019 International Conference on Computing, Networking and Communications (ICNC), Honolulu, HI, USA, 2019, pp. 29-33, doi: 10.1109/ICCNC.2019.8685594.

[28]   M. Gapeyenko et al., "Analysis of human-body blockage in urban millimeter-wave cellular communications," 2016 IEEE International Conference on Communications (ICC), Kuala Lumpur, 2016, pp. 1-7, doi: 10.1109/ICC.2016.7511572.

[29]   M. Gapeyenko, I. Bor-Yaliniz, S. Andreev, H. Yanikomeroglu and Y. Koucheryavy, "Effects of Blockage in Deploying mmWave Drone Base Stations for 5G Networks and Beyond," 2018 IEEE International Conference on Communications Workshops (ICC Workshops), Kansas City, MO, 2018, pp. 1-6, doi: 10.1109/ICCW.2018.8403671.

[30]   C. Slezak, V. Semkin, S. Andreev, Y. Koucheryavy and S. Rangan, "Empirical Effects of Dynamic Human-Body Blockage in 60 GHz Communications," in IEEE Communications Magazine, vol. 56, no. 12, pp. 60-66, December 2018, doi: 10.1109/MCOM.2018.1800232.

[31]   I. A. Hemadeh, K. Satyanarayana, M. El-Hajjar and L. Hanzo, "Millimeter-Wave Communications: Physical Channel Models, Design Considerations, Antenna Constructions, and Link-Budget," in IEEE Communications Surveys & Tutorials, vol. 20, no. 2, pp. 870-913, Secondquarter 2018, doi: 10.1109/COMST.2017.2783541.

[32]   E. Bjornson, L. Van der Perre, S. Buzzi and E. G. Larsson, "Massive MIMO in Sub-6 GHz and mmWave: Physical, Practical, and Use-Case Differences," in IEEE Wireless Communications, vol. 26, no. 2, pp. 100-108, April 2019, doi: 10.1109/MWC.2018.1800140.

[33]   S. Rangan, T. S. Rappaport and E. Erkip, "Millimeter-Wave Cellular Wireless Networks: Potentials and Challenges," in Proceedings of the IEEE, vol. 102, no. 3, pp. 366-385, March 2014, doi: 10.1109/JPROC.2014.2299397.

[34]   Z. Pi and F. Khan, "System design and network architecture for a millimeter-wave mobile broadband (MMB) system," 34th IEEE Sarnoff Symposium, Princeton, NJ, 2011, pp. 1-6, doi: 10.1109/SARNOF.2011.5876444.

[35]   M. N. U. Rajan and A. V. Babu, "Theoretical maximum throughput of IEEE 802.11ad millimeter wave wireless LAN in the contention based access period: With two level aggregation," 2017 International Conference on Wireless Communications, Signal Processing and Networking (WiSPNET), Chennai, 2017, pp. 2531-2536, doi: 10.1109/WiSPNET.2017.8300218.

[36]   H. Q. Ngo and E. G. Larsson, "No Downlink Pilots Are Needed in TDD Massive MIMO," in IEEE Transactions on Wireless Communications, vol. 16, no. 5, pp. 2921-2935, May 2017, doi: 10.1109/TWC.2017.2672540.

[37]   H. Q. Ngo, E. G. Larsson and T. L. Marzetta, "Aspects of favorable propagation in Massive MIMO," 2014 22nd European Signal Processing Conference (EUSIPCO), Lisbon, 2014, pp. 76-80.

[38]   P. S. Suratia and S. K. Shah, "Performance analysis of Open and Closed Loop Spatial Multiplexing in LTE Downlink Physical Layer," 2012 IEEE International Conference on Communication, Networks and Satellite (ComNetSat), Bali, 2012, pp. 60-63, doi: 10.1109/ComNetSat.2012.6380777.

[39] H. Q. Ngo, A. Ashikhmin, H. Yang, E. G. Larsson and T. L. Marzetta, "Cell-Free Massive MIMO: Uniformly great service for everyone," 2015 IEEE 16th International Workshop on Signal Processing Advances in Wireless Communications (SPAWC), Stockholm, 2015, pp. 201-205, doi: 10.1109/SPAWC.2015.7227028.

[40] S. Buzzi and C. D'Andrea, "Cell-Free Massive MIMO: User-Centric Approach," in IEEE Wireless Communications Letters, vol. 6, no. 6, pp. 706-709, Dec. 2017, doi: 10.1109/LWC.2017.2734893.

[41] C. Gustafson and F. Tufvesson, "Characterization of 60 GHz shadowing by human bodies and simple phantoms," 2012 6th European Conference on Antennas and Propagation (EUCAP), Prague, 2012, pp. 473-477, doi: 10.1109/EuCAP.2012.6206265.

[42] J. S. Lu, D. Steinbach, P. Cabrol and P. Pietraski, "Modeling human blockers in millimeter wave radio links", ZTE Commun., vol. 10, no. 4, pp. 23-28, Dec. 2012.

[43] The University of Florida Academic Health Center. "Event Planning Guidelines: Room Setup." [Online] [Cited: 8th August 2020.] https://events.health.ufl.edu/ufhealtheventstaff/planning-guidelines/room-setup/.

[44] WILLEN, Carin; LEHMANN, Kirsten; SUNNERHAGEN, Katharina. "Walking speed indoors and outdoors in healthy persons and in persons with late effects of polio." Journal of Neurology Research, 2013, vol. 3, no 2, p. 62-67.

[45] SERIES, M. "Guidelines for evaluation of radio interface technologies for IMT-2020." 2017.

[46] 3GPP, "Study on licensed-assisted access to unlicensed spectrum," 3GPP TR. 36.889 v13.0.0., Jun. 2015.

[47] First in Architecture. "Metric Data 02: Average dimensions of man and woman sitting." [Online] [Cited: 10th August 2020.] https://www.firstinarchitecture.co.uk/metric-data-02-average-dimensions-of-person-sitting/.

[48] J. Kibiłda et al., "Indoor Millimeter-Wave Systems: Design and Performance Evaluation," in Proceedings of the IEEE, vol. 108, no. 6, pp. 923-944, June 2020, doi: 10.1109/JPROC.2020.2989189.

7 ANNEXES

7.1 USER MOBILITY CODE

```
function [UE_position, UE_motion_azimuth] = UE_mobility_mod4
(UE_speed_interval , total_time, time_step, slot_gap, x_boundaries,
y_boundaries, num_UE, x_UE_initial, y_UE_initial,time_steps_cont_move,...
    x_gap_start, y_gap_start, x_gap_end, y_gap_end)

%INPUTS:

%UE_speed_interval: array containing the minimum and maximum speed [m/s] at
which
%the UE is desired to move (for fixed speed, repeat the speed value twice)

%total_time: total time of the simulation [s]

%time_step: step at which time is considered in the simulation [s]

%slot_gap: number of time steps that are skipped between each actually
%simulated slot

%x_boundaries: array containing the minimum and maximum x dimension [m]

%y_boundaries: array containing the minimum and maximum y dimension [m]

%num_UE: number of UEs

%x_UE_initial: array containing the initial x coordinates of the UEs

%y_UE_initial: array containing the initial y coordinates of the UEs

%time_steps_cont_move: accounts for the time steps in which the speed and
%direction of movement of the UEs remains unchanged

%x_gap_start: starting x coordinate of the gap

%y_gap_start: starting y coordinate of the gap

%x_gap_end: ending x coordinate of the gap

%y_gap_end: ending y coordinate of the gap

%If there is a gap, it means that users will not be within it at any given
%time, so it is relevant to assure that the initial positions are also out
%of the mentioned gap

%OUTPUTS:

%UE_position: array containing the position of the UE for each of the
%actually simulated slots

%UE_motion_azimuth: array containing the angle relative to the x axis whith
%which UEs are moving for each of the actually simulated slots

%Now, all relevant variables are initialised
s_min = UE_speed_interval (1);
s_max = UE_speed_interval (2);
x_UE_mob = zeros(num_UE,total_time/(time_step*slot_gap));
```

```matlab
x_UE_mob(:,1) = x_UE_initial;
y_UE_mob = zeros(num_UE,total_time/(time_step*slot_gap));
y_UE_mob(:,1) = y_UE_initial;
UE_position = zeros(num_UE,2*total_time/(time_step*slot_gap));
UE_position(:,1) = x_UE_initial;
UE_position(:,2) = y_UE_initial;
x_min = x_boundaries(1);
x_max = x_boundaries(2);
y_min = y_boundaries(1);
y_max = y_boundaries(2);
spd = zeros (num_UE,1);
dir = zeros (num_UE,1);
UE_motion_azimuth = zeros (num_UE,total_time/(time_step*slot_gap));
count = time_steps_cont_move/slot_gap;
j=1;
k=1;
for t = 0+time_step:time_step*slot_gap:total_time
    j=j+2;
    k=k+1;
    for i = 1:num_UE
        if(count==time_steps_cont_move/slot_gap) %count keeps the speed and
direction frozen for the desired time (time_steps_cont_move/slot_gap)
            spd(i) = unifrnd (s_min,s_max);
            dir(i) = unifrnd (0,2*pi()); %direction is randomly generated for
each UE when unfrozen
            UE_motion_azimuth (i,t-time_step+1) = dir(i);
        else
            UE_motion_azimuth (i,t-time_step+1) = UE_motion_azimuth
(i,int32(t-time_step));
        end
        despl_x = cos(dir(i))*spd(i)*time_step*slot_gap;
        despl_y = sin(dir(i))*spd(i)*time_step*slot_gap;
        %Now, boundaries and gap constraints are applied, and the new position
        %is stored if it complies with the contrains. If not, the previous
        %position is stored.
        if((x_min<(x_UE_mob(i,k-1)+despl_x))...
                &&((x_UE_mob(i,k-1)+despl_x)<x_max)...
                &&(y_min<(y_UE_mob(i,k-1)+despl_y))...
                &&((y_UE_mob(i,k-1)+despl_y)<y_max)...
                &&(((x_UE_mob(i,k-1)+despl_x)<x_gap_start)...
                ||((x_UE_mob(i,k-1)+despl_x)>x_gap_end)...
                ||((y_UE_mob(i,k-1)+despl_y)<y_gap_start)...
                ||((y_UE_mob(i,k-1)+despl_y)>y_gap_end)))
            UE_position(i,j)=x_UE_mob(i,k-1)+despl_x;
            UE_position(i,j+1)=y_UE_mob(i,k-1)+despl_y;
            x_UE_mob(i,k)=x_UE_mob(i,k-1)+despl_x;
            y_UE_mob(i,k)=y_UE_mob(i,k-1)+despl_y;
        else
            UE_position(i,j)=x_UE_mob(i,k-1);
            UE_position(i,j+1)=y_UE_mob(i,k-1);
            x_UE_mob(i,k)=x_UE_mob(i,k-1);
            y_UE_mob(i,k)=y_UE_mob(i,k-1);
        end
    end
    if (count<time_steps_cont_move/slot_gap)
        count = count+1;
    else
        count = 1;
    end
end
end
```

7.2 BODY BLOCKAGE CODE

```matlab
function [L] = body_blockage_model_3GPP_AoA (UE_motion_azimuth, UE_pos,
AP_pos, AoA_path_deg, height_UE, body_height)

%UE_motion_azimuth: relative azimuth to x axis of the UE orientation/motion
direction

%UE_pos: user equipment position

%AP_pos: access point position

%AoA_path_deg: angle of arrival in degrees

%height_UE: user equipment height

%body_height: user height

body_width = 0.3; %3GPP
dst_body_UE = 0.2 + body_width/2; %Distance between the UE and the user
(taking into account that the user's body is modelled as a cylinder of 0.3 m
of diameter)
AP_height = 4; %Access point height [m]
freq = 60e9; %Frequency [Hz]
lambda = physconst('LightSpeed')/freq; %Wavelength [m]

while(AoA_path_deg<0)
    AoA_path_deg = AoA_path_deg + 360;
end
while(AoA_path_deg>360)
    AoA_path_deg = AoA_path_deg - 360;
end
AoA_path_rad = AoA_path_deg*pi()/180;

if (AoA_path_rad>=0&&AoA_path_rad<=pi()/2)
    compl_angle = pi()/2 - AoA_path_rad;
    body_pos_1 = [UE_pos(1)-
dst_body_UE*cos(AoA_path_rad)+(body_width/2)*cos(compl_angle) UE_pos(2)-
dst_body_UE*sin(AoA_path_rad)-(body_width/2)*sin(compl_angle)];
    body_pos_2 = [UE_pos(1)-dst_body_UE*cos(AoA_path_rad)-
(body_width/2)*cos(compl_angle) UE_pos(2)-
dst_body_UE*sin(AoA_path_rad)+(body_width/2)*sin(compl_angle)];
    body_pos_3_AoA = [UE_pos(1)-dst_body_UE*cos(AoA_path_rad) UE_pos(2)-
dst_body_UE*sin(AoA_path_rad)];
    body_pos_1 = body_pos_1 - body_pos_3_AoA + body_pos_3;
    body_pos_2 = body_pos_2 - body_pos_3_AoA + body_pos_3;
elseif(AoA_path_rad>(pi()/2)&&AoA_path_rad<=pi())
    compl_angle = AoA_path_rad - pi()/2;
    compl_angle_UE = pi() - AoA_path_rad;
    body_pos_1 =
[UE_pos(1)+dst_body_UE*cos(compl_angle_UE)+(body_width/2)*cos(compl_angle)
UE_pos(2)-dst_body_UE*sin(compl_angle_UE)+(body_width/2)*sin(compl_angle)];
    body_pos_2 = [UE_pos(1)+dst_body_UE*cos(compl_angle_UE)-
(body_width/2)*cos(compl_angle) UE_pos(2)-dst_body_UE*sin(compl_angle_UE)-
(body_width/2)*sin(compl_angle)];
    body_pos_3_AoA = [UE_pos(1)+dst_body_UE*cos(compl_angle_UE) UE_pos(2)-
dst_body_UE*sin(compl_angle_UE)];
    body_pos_1 = body_pos_1 - body_pos_3_AoA + body_pos_3;
    body_pos_2 = body_pos_2 - body_pos_3_AoA + body_pos_3;
elseif(AoA_path_rad>pi()&&AoA_path_rad<=(3*pi()/2))
    compl_angle_UE = AoA_path_rad - pi();
```

```matlab
    compl_angle = pi()/2 - compl_angle_UE;
    body_pos_1 = [UE_pos(1)+dst_body_UE*cos(compl_angle_UE)-
(body_width/2)*cos(compl_angle)
UE_pos(2)+dst_body_UE*sin(compl_angle_UE)+(body_width/2)*sin(compl_angle)];
    body_pos_2 =
[UE_pos(1)+dst_body_UE*cos(compl_angle_UE)+(body_width/2)*cos(compl_angle)
UE_pos(2)+dst_body_UE*sin(compl_angle_UE)-(body_width/2)*sin(compl_angle)];
    body_pos_3_AoA = [UE_pos(1)+dst_body_UE*cos(compl_angle_UE)
UE_pos(2)+dst_body_UE*sin(compl_angle_UE)];
    body_pos_1 = body_pos_1 - body_pos_3_AoA + body_pos_3;
    body_pos_2 = body_pos_2 - body_pos_3_AoA + body_pos_3;
elseif(AoA_path_rad>(3*pi()/2)&&AoA_path_rad<=2*pi())
    compl_angle_UE = AoA_path_rad -3*pi()/2;
    compl_angle = pi()/2 - compl_angle_UE;
    body_pos_1 = [UE_pos(1)-dst_body_UE*cos(compl_angle_UE)-
(body_width/2)*cos(compl_angle) UE_pos(2)+dst_body_UE*sin(compl_angle_UE)-
(body_width/2)*sin(compl_angle)];
    body_pos_2 = [UE_pos(1)-
dst_body_UE*cos(compl_angle_UE)+(body_width/2)*cos(compl_angle)
UE_pos(2)+dst_body_UE*sin(compl_angle_UE)+(body_width/2)*sin(compl_angle)];
    body_pos_3_AoA = [UE_pos(1)-dst_body_UE*cos(compl_angle_UE)
UE_pos(2)+dst_body_UE*sin(compl_angle_UE)];
    body_pos_1 = body_pos_1 - body_pos_3_AoA + body_pos_3;
    body_pos_2 = body_pos_2 - body_pos_3_AoA + body_pos_3;
end

%body_pos_1/2/3 are body positions relative to the top view

%body_pos_1 is the position of the end of the body that forms a relative
%angle of +90° with the AoA

%body_pos_2 is the position of the end of the body that forms a relative
%angle of -90° with the AoA

%body_pos_3 is the position of the end of center of the body, which forms
%a relative angle of 0° with the AoA

%D1w1 y D1w2 are the distances (top view) from the UE to each end of the body
D1w1 = sqrt((body_pos_1(1)-UE_pos(1))^2+(body_pos_1(2)-UE_pos(2))^2);
D1w2 = sqrt((body_pos_2(1)-UE_pos(1))^2+(body_pos_2(2)-UE_pos(2))^2);
%D2w1 y D2w2 are the distances (top view) from the AP to each end of the body
D2w1 = sqrt((body_pos_1(1)-AP_pos(1))^2+(body_pos_1(2)-AP_pos(2))^2);
D2w2 = sqrt((body_pos_2(1)-AP_pos(1))^2+(body_pos_2(2)-AP_pos(2))^2);
%D1h1 y D1h2 are the distances (side view) from the UE to each end of the body
D1h1 = sqrt((body_height-height_UE)^2+dst_body_UE^2);
D1h2 = sqrt(height_UE^2+dst_body_UE^2);
%D1h1 y D1h2 are the distances (side view) from the AP to each end of the body
D2h1 = sqrt((body_pos_3(1)-AP_pos(1))^2+(body_pos_3(2)-
AP_pos(2))^2+(body_height-AP_height)^2);
D2h2 = sqrt((body_pos_3(1)-AP_pos(1))^2+(body_pos_3(2)-
AP_pos(2))^2+AP_height^2);

%Now, the angle that forms the UE orientation/motion direction with the
%straight line between the UE and the AP is obtained. If this angle is
%equal or higher than 128.66° (intercept_top_angle), it will be considered
%that, from the top view standpoint, there is line of sight interruption,
%so top_intercept will be equal to 1

%intercept_top_angle is the angle between the UE orientation/motion
%direction and the straight line between the UE and the AP where the end of
%the body is aligned with the straight line between the UE and the AP, from
%a top view standpoint
```

35

```matlab
intercept_top_angle = ((pi()/2)-atan((body_width/2)/dst_body_UE))*180/pi()+90;
UE_motion_dir = [cos(UE_motion_azimuth) sin(UE_motion_azimuth)];
UE_AP_dir = [AP_pos(1)-UE_pos(1) AP_pos(2)-UE_pos(2)];
UE_AP_dir_norm = UE_AP_dir/norm(UE_AP_dir);
UE_AP_dirs_angle = acos
(UE_motion_dir(1)*UE_AP_dir_norm(1)+UE_motion_dir(2)*UE_AP_dir_norm(2));
UE_AP_dirs_angle_deg = UE_AP_dirs_angle*180/pi();

if (UE_AP_dirs_angle_deg<intercept_top_angle)
    top_intercept = 0;
else
    top_intercept = 1;
end

%Now, it is checked if there is line of sight interruption by the body in
%the side plane. In order to do so, the distance between the UE and the
%AP from which there will be such interruption
%(intercept_UE_AP_2d_distance) and, therefore, side_intercept will be equal
%to 1
%It is considered that, if there is not line of sight interruption from the
%top view standpoint, there will not be interruption from the side plane
%standpoint either, so side_intercept will be equal to 0 if top_intercept
%is equal to 0

intercept_side_angle = atan((body_height-height_UE)/dst_body_UE);
intercept_UE_AP_2d_distance = (AP_height-height_UE)/tan(intercept_side_angle);

if (top_intercept == 1)
    dist_UE_AP_2d = sqrt((AP_pos(1)-UE_pos(1))^2+(AP_pos(2)-UE_pos(2))^2);
    if(dist_UE_AP_2d<intercept_UE_AP_2d_distance) %2.5 m para una altura de
los AP de 4 m, altura del UE de 1.5 m, altura de la persona de 1.7 m y una
distancia horizontal entre UE y persona de 20 cm
        side_intercept = 0;
    else
        side_intercept = 1;
    end
else
    side_intercept = 0;
end

%Having determined whether or not is there line of sight interruption
%because of the body from the top and side views standpoints, equations
%are written according to the 3GPP recommendation, using the line of sight
%variant because, apart from body blockage, in the considered scenario, due
%to it being an open space, only line of sight propagation occurs. Also,
%the necessary elements for the equations, namely the size of the straight
%lines between the AP and UE for the top view (r_2d) and the side view
%(r_3d) are calculated

%So, for each plane, in case there is line of sight interruption because of
%the body, the sign + is used for both equations of each pair. If there is
%not any interruption, then the sign - is used for the equation corresponding
%to the shortest of the two paths that exist between the UE, each end of the
%body, and the AP, and sign + is used for the equation corresponding to the
%longest path

r_2d = sqrt((UE_pos(1)-AP_pos(1))^2+(UE_pos(2)-AP_pos(2))^2);
r_3d = sqrt((UE_pos(1)-AP_pos(1))^2+(UE_pos(2)-AP_pos(2))^2+(height_UE-
AP_height)^2);

%With the following lines, errors caused because of the finite precision of
%MATLAB that resulted in undesired complex values are avoided
```

36

```matlab
D1h1 = round(D1h1,4);
D2h1 = round(D2h1,4);
D1h2 = round(D1h2,4);
D2h2 = round(D2h2,4);
D1w1 = round(D1w1,4);
D2w1 = round(D2w1,4);
D1w2 = round(D1w2,4);
D2w2 = round(D2w2,4);
r_2d = round(r_2d,4);
r_3d = round(r_3d,4);

if(side_intercept==0)
    if((D1h1+D2h1)<(D1h2+D2h2))
        Fh1 = atan((-pi()/2)*sqrt((pi()/lambda)*(D1h1+D2h1-r_3d)))/pi();
        Fh2 = atan((+pi()/2)*sqrt((pi()/lambda)*(D1h2+D2h2-r_3d)))/pi();
    else
        Fh1 = atan((+pi()/2)*sqrt((pi()/lambda)*(D1h1+D2h1-r_3d)))/pi();
        Fh2 = atan((-pi()/2)*sqrt((pi()/lambda)*(D1h2+D2h2-r_3d)))/pi();
    end
else
    Fh1 = atan((+pi()/2)*sqrt((pi()/lambda)*(D1h1+D2h1-r_3d)))/pi();
    Fh2 = atan((+pi()/2)*sqrt((pi()/lambda)*(D1h2+D2h2-r_3d)))/pi();
end

if(top_intercept==0)
    if((D1w1+D2w1)<(D1w2+D2w2))
        Fw1 = atan((-pi()/2)*sqrt((pi()/lambda)*(D1w1+D2w1-r_2d)))/pi();
        Fw2 = atan((+pi()/2)*sqrt((pi()/lambda)*(D1w2+D2w2-r_2d)))/pi();
    else
        Fw1 = atan((+pi()/2)*sqrt((pi()/lambda)*(D1w1+D2w1-r_2d)))/pi();
        Fw2 = atan((-pi()/2)*sqrt((pi()/lambda)*(D1w2+D2w2-r_2d)))/pi();
    end
else
    Fw1 = atan((+pi()/2)*sqrt((pi()/lambda)*(D1w1+D2w1-r_2d)))/pi();
    Fw2 = atan((+pi()/2)*sqrt((pi()/lambda)*(D1w2+D2w2-r_2d)))/pi();
end

L = 20*log10(1-(Fh1+Fh2)*(Fw1+Fw2)); %Body blockage losses [dB]
L = 10^(L/10); %Body blockage losses [linear units]
end
```